

INCORPORATION OF DIRECTIONALLY DEPENDANT
DIFFUSION WITH POLYMER COMPOSITE FLOW THEORY

A Thesis presented to
the Faculty of the Graduate School
University of Missouri - Columbia

In Partial Fulfillment
of the Requirements for the Degree

Master of Science

by
DAVID ABRAM JACK

Dr. Stephen Montgomery-Smith, Thesis Supervisor

DECEMBER 2006

©Copyright by David Abram Jack 2006
All Rights Reserved

The undersigned, appointed by the Dean of the Graduate School, have examined the thesis entitled

INCORPORATION OF DIRECTIONALLY DEPENDANT
DIFFUSION WITH POLYMER COMPOSITE FLOW THEORY

Presented by David Abram Jack, a candidate for the degree of Master of Science, and hereby certify that in their opinion it is worthy of acceptance.

Dr. Stephen Montgomery-Smith

Dr. Carmen Chicone

Dr. Douglas E. Smith

*To my best friend and dear wife Trisha, who has patiently let me
pursue my varied research interests.*

ACKNOWLEDGEMENTS

Research is never undertaken in seclusion, but is always a team effort. Without the support, guidance, and motivation of others, the following work would never have been completed. I am sincerely grateful for each of those who have provided me assistance and support.

Dr. Stephen Montgomery-Smith has been an invaluable resource. He has patiently taught me the importance of a strong mathematical foundation upon which to build applicable theories of physical processes. He has spent many long hours listening to my thoughts, and is adept enough to quickly find fault and provide solutions for engineering problems. He has also provided personal guidance, both in my career and in my personal life. I am exceedingly grateful for both.

I want to thank my advisor from Mechanical and Aerospace Engineering, Dr. Douglas E. Smith. When I approached him suggesting I wanted to pursue an Applied Mathematics degree in addition to the work I was doing for him toward my Ph.D. in Mechanical and Aerospace Engineering, he encouraged me. He understood that it would take away from my doctoral research, but in the long run would be beneficial to myself in my future endeavors. It was his initial insight that has provided the spark for the present work, and much credit must be given to him for his ability to grasp the greater picture. He has provided me with direction, both in my research and my career, for which I will be forever indebted.

I would also like to thank Dr. Carmen Chicone. His advice and patience with this simple engineer have made the present work stronger.

I would like to thank the GAANN program of the United States Department of Education for providing the financial means to complete this work.

I save my most heartfelt appreciation for my best friend and dear wife, Trisha. Without her understanding nature, patience, and caring, I would never have come this far. She makes the whole process enjoyable and is genuinely a gift from God.

TABLE OF CONTENTS

Acknowledgements	ii
List of Figures	v
Abstract	viii
Chapter 1 Introduction	1
Chapter 2 Fiber Orientation Kinematics	8
2.1 Representation of Fiber Orientation	8
2.2 Dynamics of Fiber Orientation	16
2.3 Current Models for Rotary Diffusivity in Short-Fiber Polymer Com- posite Processes	19
Chapter 3 Incorporation of Directionally Dependant Diffusion	23
3.1 General Form for Directionally Dependant Diffusion	23
3.2 Orientation Tensor Evolution	25
3.2.1 Spherical Coordinate Representation	27
3.2.2 Equation of Change for $\mathbf{B}(\mathbf{r}) = \mathbf{r}\mathbf{r}$	28
3.2.2.1 Equation of Change: Jeffery's Equation	30
3.2.2.2 Equation of Change: Directionally Dependant Diffusion	33
Chapter 4 Directionally Dependant Diffusion Models	35
4.1 Preliminary Model for First-Order Directionally Dependant Diffusion	36

4.1.1	Graphical Description for First-Order Model	37
4.1.2	Orientation Tensor Evolution Formulation and Results	38
4.1.3	Orientation Tensor Evolution Results	42
4.1.3.1	Results for $D_2 = -10^{-1}$: Simple Shear Flow	44
4.1.3.2	Results for $D_1 = D_1(D_2)$: Simple Shear Flow	46
4.1.3.3	Results for $D_1 = D_1(D_2)$: Uniaxial Elongation Flow	48
4.1.4	Impediment for Preliminary Diffusion Model	48
4.2	Advanced Model for Directional Diffusion	51
4.2.1	Development of Advanced Directional Diffusion Model	51
4.2.2	Orientation Tensor Evolution Formulation	58
4.2.3	Orientation Tensor Evolution Closure Selection	60
4.2.4	Orientation Tensor Evolution Results	62
4.2.4.1	Simple Shear Flow	63
4.2.4.2	Uniaxial Elongation Flow	69
4.2.4.3	Combined Shearing and Elongational Flow	71
Chapter 5	Conclusions and Future Work	76
Bibliography	79
Vita	86

LIST OF FIGURES

2.1	Coordinate system defining the unit vector $\mathbf{r}(\theta, \phi)$ along with the angles θ and ϕ	9
2.2	Isotropic orientation state, $\psi(\theta, \phi) = \frac{1}{4\pi}$	15
2.3	Uniaxially aligned orientation state along x_1 axis.	15
3.1	Single fiber within an isotropic 2-D fiber distribution.	26
3.2	Single fiber within a highly aligned 2-D fiber distribution.	26
4.1	First-order directionally dependant diffusion, $D_r(\theta, \phi)$, for isotropic fiber orientation state, $\psi(\theta, \phi) = \frac{1}{4\pi}$ (normalized with $\ \dot{\gamma}\ = 1$).	39
4.2	First-order directionally dependant diffusion, $D_r(\theta, \phi)$, for uniaxial fiber alignment along the x_1 axis (normalized with $\ \dot{\gamma}\ = 1$).	39
4.3	Directionally dependant diffusion for randomly orientated fiber distribution in the $x_1 - x_2$ plane (normalized with $\ \dot{\gamma}\ = 1$).	40
4.4	Eigenspace of possible orientations of the second-order orientation tensor.	43
4.5	Schematic of simple shear flow with shearing in the x_3 direction along the x_1 axis.	47
4.6	Results from simple-shear flow demonstrating steady state results for $D_1 = 8.85 \times 10^{-2}$ and $D_2 = 10^{-1}$	47
4.7	Results demonstrating the excellent correlation between optimal relation for D_1 given D_2 and linear least squares fit from simple shear flow.	49

4.8	Results demonstrating the excellent correlation between optimal relation for D_1 given D_2 and linear least squares fit from uniaxial elongation flow.	49
4.9	Coordinate system describing the path through which the fiber ρ passes into and \mathbf{r}	55
4.10	Comparison between $f(x) = x $ and $g(x) = x^2$ for $x \in [-1, 1]$	55
4.11	Transient solution for A_{ij} from the Folgar and Tucker model in simple shear flow, $v_1 = Gx_3$, $v_2 = v_3 = 0$ starting from an isotropic orientation state, $\psi(\theta, \phi) = \frac{1}{4\pi}$, for $C_I = 10^{-2}$	64
4.12	Transient solution for A_{ij} from the advanced diffusion model in simple shear flow, $v_1 = Gx_3$, $v_2 = v_3 = 0$ starting from an isotropic orientation state, $\psi(\theta, \phi) = \frac{1}{4\pi}$, with $0 \leq C_1 \leq 4$ and $C_2 = 10^{-2}$	66
4.13	Percentage difference between steady state orientation and transient orientation state for A_{11} in simple shear flow, $v_1 = Gx_3$, $v_2 = v_3 = 0$ starting from an isotropic orientation state, $\psi(\theta, \phi) = \frac{1}{4\pi}$, with $0 \leq C_1 \leq 4$ and $C_2 = 10^{-2}$	68
4.14	Transient solution for A_{ij} from advanced diffusion model in simple shear flow, $v_1 = Gx_3$, $v_2 = v_3 = 0$ starting from a highly aligned orientation state $A_{11} = 1 - 10^{-8}$, $A_{22} = A_{33} = \frac{1}{2} \times 10^{-8}$ and $A_{ij} = 0 \forall i \neq j$	70

4.15	Transient solution for A_{ij} from the advanced diffusion model in uniaxial elongational flow, $v_1 = 2Gx_1$, $v_2 = -Gx_2$ and $v_3 = -Gx_3$ starting from an isotropic orientation state, $\psi(\theta, \phi) = \frac{1}{4\pi}$, with $0 \leq C_1 \leq 4$ and $C_2 = 10^{-2}$	72
4.16	Percentage difference between steady state orientation and transient orientation state for A_{11} in uniaxial elongation flow, $v_1 = 2Gx_1$, $v_2 = -Gx_2$ and $v_3 = -Gx_3$ starting from an isotropic orientation state, $\psi(\theta, \phi) = \frac{1}{4\pi}$, with $0 \leq C_1 \leq 2$ and $C_2 = 10^{-2}$	73
4.17	Transient solution for A_{ij} from the advanced diffusion model for combined shearing and elongational flow, $v_1 = Gx_2 - Gx_1$, $v_2 = -Gx_2$ and $v_3 = 2Gx_3$ starting from an isotropic orientation state, $\psi(\theta, \phi) = \frac{1}{4\pi}$, with $0 \leq C_1 \leq 2$ and $C_2 = 10^{-2}$	75

INCORPORATION OF DIRECTIONALLY DEPENDANT DIFFUSION WITH POLYMER COMPOSITE FLOW THEORY

David Abram Jack

Dr. Stephen Montgomery-Smith, Thesis Supervisor

ABSTRACT

viii The extensive use of short-fiber reinforced polymer composites for industrial applications demands an accurate understanding of the fiber orientation kinematics. There is a growing concern in recent literature with the popular Folgar and Tucker (1984) model for the transient analysis of fiber orientation. As the reliability and repeatability of the material behavior from the fabrication procedure advances, the demand for accurate models for use in design processes beyond the current methods has become increasingly important.

A model to incorporate the directional nature of fiber interactions through the introduction of directional diffusion is presented based upon the observation made by Folgar and Tucker in their original work that fiber motions for concentrated suspensions are different for random orientations versus aligned orientations. This work develops the fiber orientation tensor flow equations based upon a directionally dependant diffusion model similar to that of Bird *et al.* (1987), and introduces two models for directional diffusion. The first model is readily implemented in industrial applications with the current understanding of orientation tensors, while failing to attain all of the desired characteristics. The second, advanced, model for directional diffusion provides all required attributes both in the transient solution and the steady state orientation results of the fiber distribution at the cost of requiring the orientation tensors up to the tenth-order. Future work will need to incorporate experimental results with the proposed model to refine the scalable parameters of the advanced diffusion model to produce acceptable results for industrial applications.

CHAPTER 1

INTRODUCTION

Short-fiber polymer composites have experienced widespread use in industrial fabrication processes due in large part to their high strength to weight ratio. In these products, the orientation state of the short-fibers within the polymer matrix defines the material properties of the composite structure. Therefore understanding and predicting fiber orientation during mold filling is necessary for product and process analysis and design.

Most fiber orientation analysis methods are based upon the model presented by Folgar and Tucker [1] which includes a phenomenological diffusion term to account for interactions between fibers in the polymer melt. Unfortunately, the method proposed by Folgar and Tucker employing the fiber orientation probability distribution function is limited to simple flow simulations due to excessive computational time and memory requirements (see e.g. [2, 3]). More recently, Chiba *et al.* [4] developed a computationally efficient statistical approach for modeling single non-interacting fibers along streamlines to evaluate the fiber orientation probability distribution function of non-interacting discrete fibers using Jeffery's Equation [5]. For the case of fiber-fiber interactions, Advani and Tucker [2] extended the usefulness of the Folgar and Tucker model by introducing orientation tensors to characterize the fiber orientation state using moments of the fiber orientation probability distribution function in a computationally efficient manner, even in complex flow fields. Unfortunately, the solution

for each even-ordered tensor requires the next higher even-ordered tensor. Therefore, to solve the orientation tensor evolution equation [6], a closure is required whereby higher-ordered orientation tensors are approximated as functions of lower-ordered orientation tensors. There exist many closures of the fourth-order orientation tensor in the literature [7–19], and recently, the sixth-order closures [20–22] have been receiving attention due to their effectiveness in modeling both the orientation distribution function of fibers and advanced material properties [23]. Additionally, it has been shown that the fourth-order orientation tensor plays a strong role in approximating the expectation value of fiber distributions (see e.g. [2,6,24–27]). Recently it has been demonstrated that orientation tensors up to the eighth-order [27,28] are necessary to develop the variance of the material stiffness tensor associated with a given fiber orientation probability distribution function.

Current approaches to model fiber orientation while incorporating fiber interaction effects are based upon the Folgar and Tucker model [1]. The Folgar and Tucker model introduces interaction between fibers through forces similar to Brownian motion where each of the fibers experience small forces as they collide within the suspension causing induced torques upon each ellipsoid. Folgar and Tucker propose a diffusivity function based solely upon the rate of deformation tensor and an empirically derived parameter termed the interaction coefficient. The Folgar and Tucker model does not take into account the directional dependence of the collisions notwithstanding the suggestion by Folgar and Tucker that “...while it is possible, and even likely, that these orientation changes have a directional bias, or are different in nearly

random and nearly aligned suspensions, we have chosen to ignore these features.” Their model yields exceptional results compared to previous theories, and has been considered the standard throughout both the industrial and academic communities. It has been suggested that the Folgar and Tucker model will significantly over predict the degree of orientation throughout the transient solution [29]. With recent industrial demands for efficient and accurate production design and advances in repeatable production processes, it is necessary to ensure that accurate models exist to represent the orientation state.

A comprehensive treatment of fiber suspension flow in complex geometries involves flow/orientation coupling. It is well understood that fibers orient in response to flow kinematics, while the suspension rheology is defined in part by the concentration and orientation of the suspended fibers. For example, Dinh and Armstrong [30] provide a rheological equation of state for semi-concentrated suspensions of stiff fibers in a Newtonian solvent. Flow simulations that incorporate flow/orientation coupling further emphasize the need for including these fully coupled evaluations to make accurate predictions in certain geometries. Lipscomb, et al., [8] showed that the size of the corner vortex in axisymmetric contraction changed significantly when fibers were added, and VerWeyst and Tucker [31] exposed the influence of fiber concentration on flow near the gate of an injection molded part.

In the same simulations, however, VerWeyst and Tucker [31] demonstrated that the influence of flow/orientation coupling decays rapidly with increasing distance from the gate. This latter result supports the earlier conclusion by Tucker [32] that flow

and fiber orientation evaluations may be decoupled for flows in narrow gaps where the lubrication approximation applies. Accordingly, throughout the present work the effect of fiber orientation upon the flow kinematics will be neglected to retain the focus solely upon the fiber orientation analysis. It is left for future investigations to pursue the full coupling between the fiber orientation analysis and the flow kinematics.

It has been well known that the Folgar and Tucker model has limited use for accurately representing the transient results for physical processes. Yamane *et al.* [33] curve fit an equation based upon volume fraction for the interaction coefficient for a given set of flow conditions, and similarly Bay [34] developed a comparable function based upon a different set of experimental data. These two forms assume the rate of fiber interactions is based solely upon the volume fraction and yet yield a range of interaction coefficients several orders of magnitude apart based upon the same set of fiber volume fractions. Phan-Thien *et al.* [35] discuss the discrepancy, and suggest the variation may be due to neglecting the fiber aspect ratio in the calculations. Phan-Thien and co-workers suggest that the collisions among fibers becomes less frequent as the fiber width decreases. The Folgar and Tucker model has been known to over predict the alignment of fibers during the transient solution [29]. Since the Folgar and Tucker is fit based upon the steady state results, it is assumed to accurately predict the steady-state results. For simple flows, Folgar and Tucker model may attain the steady state solution 2 to 3 times faster than actual experimental results indicate [29]. Until recently, this characteristic has been acceptable for industrial applications since there was significant uncertainty in the fabrication process. With a

continuing desire for high strength advanced materials with specific material response behavior it has become necessary to develop methods to accurately model both the steady state results and the transient solution of the fiber orientation probability distribution function.

There exist several models in the literature to account for fiber interaction, but these models have found only minimal acceptance for various reasons. Kamal and Mutel [36] propose a diffusivity model as a function of volume fraction that for sufficiently large enough volume fractions is independent of shear rate. This model allows a relaxation of the fiber orientation to a randomly distributed orientation steady state, contrary to the physical system in which fiber orientation experiences no relaxation without an induced deformation of the surrounding fluid. Phan-Thien *et al.* [35, 37] assume an anisotropic second-order tensor form for the diffusivity, but again neglect the directional dependence of the fiber distribution. Additionally, results are only investigated for steady state flow conditions. Phan-Thien and co-workers conclude with the remark that fiber interactions may not be best described by a simple diffusion process, but clearly the Folgar and Tucker model must be further investigated and improved upon to allow accurate simulations of fiber orientation in industrial processes. Koch [38] proposed an expression without proof or results for the orientational diffusion of a test fiber. Recently, Tucker *et al.* [29] introduced a strain reduction factor to the Folgar-Tucker model and presented preliminary results from their new model. This parameter is selectively chosen depending upon the flow conditions, and has the effect of scaling time in the flow equations. Although this model has shown promising

results, it is unclear what the model is based upon and an exhaustive study of the time scaling factor has yet to be presented in the literature.

This paper seeks to develop a procedure for developing models that have a directional dependence for diffusion, thereby incorporating the local effects of the distribution of fibers. There are two approaches to incorporate the directional nature of the fiber collisions. The first is based upon a complete understanding of the nature of the fiber collisions and will require a precise understanding of the physical nature of the collision between two fibers and should be investigated in future endeavors. Once the physical phenomena causing reorientations between densely packed fibers are fully understood, a true physical model can be formulated. The second approach, which is undertaken here, represents collisions as being locally averaged into a diffusion model. This approach is similar to that of Bird [39, 40] where for crystalline polymer flow, collision phenomena are considered to be due to diffusion. A clear development of a general diffusion model is made along with assumptions necessary for any future model belonging to the general diffusion model. Additionally, extensive consideration is made in developing the orientation tensor evolution equations to allow practical implementation for industrial use. A preliminary, first order model based upon the first- and second-moment of inertia of a single fiber is presented. The preliminary model is discarded in favor of the advanced directionally dependent diffusion model, which upon simplification of the second-order orientation tensor flow equations the advanced diffusion model is shown to require the orientation tensors up to the tenth-order. The advanced model has all the desired characteristics, and

can be easily implemented in existing flow calculations employing the second-order orientation tensor using the proposed eighth- and tenth-order moment closures. The advanced directional diffusion model provides two scalable parameters, one which contributes significantly to the steady state solution, and a second which mostly contributes to the transient behavior of the solution. Recall the currently accepted Folgar and Tucker model is fit to steady state results observed in the laboratory. Therefore, the parameter primarily affecting the steady state solution is set to produce the same steady state as the Folgar and Tucker model, and the second parameter is adjusted to diminish the rate at which the fibers align to better approximate the physical system under consideration.

CHAPTER 2

FIBER ORIENTATION KINEMATICS

Due to extensive use of short-fiber polymer composites in industrial applications, a complete understanding must be made to allow effective product and process design. This chapter sets the framework to develop effective models to analyze the flow kinematics and fiber orientation relationship. Development begins with the representation of a single fiber and transitions to the distribution of fibers necessary for effective industrial applications. Considerations such as bulk fluid deformation, fiber volume fraction, and fiber aspect ratio are incorporated with the motion of a single fiber. Lastly, a discussion of the existing diffusion models is undertaken to introduce the limitations of the existing theories.

2.1 Representation of Fiber Orientation

The orientation of a single rigid fiber within a polymer matrix can be described by the angle pair, (θ, ϕ) , or by the unit vector $\mathbf{r}(\theta, \phi)$ aligned along the axis of the fiber as shown in Figure 2.1 with the relation between the two descriptions simply being

$$\mathbf{r}(\theta, \phi) = \begin{pmatrix} \sin\theta \cos\phi \\ \sin\theta \sin\phi \\ \cos\theta \end{pmatrix} \quad (2.1)$$

Observe that a fiber along $\mathbf{r}(\theta, \phi)$ will be indistinguishable from a fiber aligned

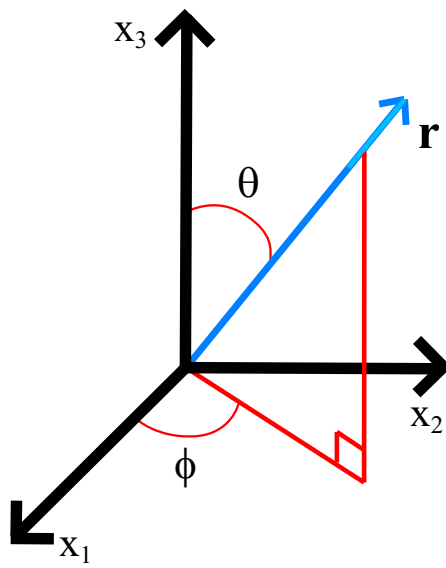


Figure 2.1: Coordinate system defining the unit vector $\mathbf{r}(\theta, \phi)$ along with the angles θ and ϕ .

along $-\mathbf{r}(\theta, \phi)$ since the two ends of the fiber are identical [41], therefore any description of the orientation must satisfy the substitutions

$$\theta \rightarrow \pi - \theta \quad \text{and} \quad \phi \rightarrow \phi + \pi \quad (2.2)$$

Fibers are rarely, if ever, perfectly aligned along a single direction, but instead each discrete fiber will have a orientation that varies from nearby fibers. There are examples where each discrete fiber has been modeled in simple flows for small numbers of fibers [35], but for typical industrial use modeling individual fibers is computationally impractical. Therefore, the discrete set of fibers is assumed to satisfy a given continuous probability distribution function $\psi(\theta, \phi)$ defined such that the probability of finding a fiber between the angles θ_i and $\theta_i + d\theta$ and between ϕ_i and $\phi_i + d\phi$ is given as [6]

$$P(\theta_i \leq \theta \leq \theta_i + d\theta, \phi_i \leq \phi \leq \phi_i + d\phi) = \psi(\theta, \phi) \sin \theta d\theta d\phi \quad (2.3)$$

Observe that Equation (2.2) will cause the distribution to be an even function, i.e.

$$\psi(\theta, \phi) = \psi(\pi - \theta, \phi + \pi) \quad (2.4)$$

Since every fiber must lie upon some angle pair $(\theta, \phi) \in \mathbb{S}^2$, the integral of the distribution function over the unit sphere \mathbb{S}^2 must be equal to one

$$\oint_{\mathbb{S}^2} \psi(\theta, \phi) d\mathbb{S}^2 = \int_0^{2\pi} \int_0^\pi \psi(\theta, \phi) \sin \theta d\theta d\phi = 1 \quad (2.5)$$

which is often referred to as the normalization condition. The distribution function is considered to be a continuous function and is assumed to vary smoothly with position [41]. The fiber distribution function $\psi(\theta, \phi)$ is a complete description, if the

orientation of a fiber is statistically uncorrelated with that of any of its neighbors. The case of “orientational clustering” has been considered by Ranganathan and Advani [42] where the local clustering of the fibers causes a local inhomogeneity of the distribution function. This phenomena is relegated to complex flow fields, and is neglected here since all results will be for simple flow fields.

The fiber orientation distribution function is a complete description of the fiber orientation state, but calculations with the distribution function are too cumbersome to apply to industrially relevant flows due to computational considerations. Additionally, $\psi(\theta, \phi)$ does not yield an easy interpretation into physical behavior [2,23,41]. An alternative approach is to consider an average orientation property over a sufficiently large enough volume to contain many fibers, but small enough such that the statistics of the orientation are uniform throughout. This assumption is valid when the volume is small in regards to the dimensions of the part but large in regards to the fiber length [43]. Let $\mathbf{B}^n(\theta, \phi)$ represent some property associated with the n^{th} fiber, then the local average for N discrete sample sets of $\{\mathbf{B}^n(\theta, \phi) : 1 \leq n \leq N, n \in \mathbb{N}, N \in \mathbb{N}\}$, denoted by $\langle \mathbf{B} \rangle$, is defined as

$$\langle \mathbf{B} \rangle = \frac{1}{N} \sum_{n=1}^N \mathbf{B}^n(\theta, \phi) \quad (2.6)$$

If the set $\{\mathbf{B}^n(\theta, \phi) : 1 \leq n \leq N\}$ is sampled from the fiber orientation probability distribution function $\psi(\theta, \phi)$, and as $N \rightarrow \infty$ the volume average of the quantity will be equal to its expected value as

$$\langle \mathbf{B} \rangle = \oint_{\mathbb{S}^2} \mathbf{B}(\theta, \phi) \psi(\theta, \phi) d\mathbb{S}^2 \quad (2.7)$$

Current practice to represent the distribution function of fibers uses the moments of the distribution function to represent the orientation state. Therefore the generality of the distribution function is cast in a compact form for rapid computations where the property $\mathbf{B}(\theta, \phi)$ is set to $\mathbf{B}(\theta, \phi) = \mathbf{r}(\theta, \phi) \mathbf{r}(\theta, \phi) \cdots$, or in index notation, $B_{ij\dots} = r_i r_j \cdots$ where r_i is the i^{th} component of the vector $\mathbf{r}(\theta, \phi)$ and the dependence of r_i upon (θ, ϕ) is understood. Here, and throughout the text, index notation along with the Einstein summation convention will be employed for simplicity. In index notation the value B_{ij} designates the i, j component of the tensor function $\mathbf{B}(\theta, \phi)$, and the Einstein summation convention simply sums upon a repeated index, i.e. $\sum_{i=1}^3 B_{ii} = B_{ii} = B_{11} + B_{22} + B_{33}$ where $i, j, k, \dots \in \{1, 2, 3\}$ since we are in \mathbb{R}^3 throughout the scope of the present work.

The moments of the distribution, commonly referred to as the orientation tensors, are defined as [2]

$$\begin{aligned}
 A_{ij} &= \oint_{\mathbb{S}^2} r_i r_j \psi(\theta, \phi) \, d\mathbb{S}^2 & A_{ijkl} &= \oint_{\mathbb{S}^2} r_i r_j r_k r_l \psi(\theta, \phi) \, d\mathbb{S}^2 \\
 A_{ij\dots} &= \oint_{\mathbb{S}^2} r_i r_j \dots \psi(\theta, \phi) \, d\mathbb{S}^2 & &
 \end{aligned} \tag{2.8}$$

Due to the symmetric nature of the fiber orientation probability distribution function, Equation (2.4), odd ordered orientation tensors integrate to zero and will not be discussed further. Through the application of Equations (2.1) and (2.8) orientation

tensors can be shown to be completely symmetric

$$\begin{aligned}
A_{ij} &= A_{ji} \\
A_{ijkl} &= A_{klij} = A_{jikl} = A_{ilkj} = \dots \\
A_{ijklmn} &= A_{jiklmn} = A_{klijmn} = A_{mnklij} = A_{ilkjmn} = A_{inklmj} = \dots
\end{aligned} \tag{2.9}$$

Note that A_{ijkl} enjoys more symmetries than those found in an anisotropic stiffness or compliance tensor (see e.g. [44,45]). In addition, higher order orientation tensors completely describe lower order orientation tensors which can be shown using the normalization condition of the distribution function $\psi(\theta, \phi)$ from Equation (2.5) along with Equation (2.1) and Equation (2.8)

$$\begin{aligned}
A_{ij\dots\alpha\beta\gamma\gamma} &= \oint_{\mathbb{S}^2} r_i r_j \dots r_\alpha r_\beta r_\gamma r_\gamma \psi(\theta, \phi) d\mathbb{S}^2 \\
&= \oint_{\mathbb{S}^2} r_i r_j \dots r_\alpha r_\beta (r_1 r_1 + r_2 r_2 + r_3 r_3) \psi(\theta, \phi) d\mathbb{S}^2 \\
&= \oint_{\mathbb{S}^2} r_i r_j \dots r_\alpha r_\beta (\|\mathbf{r}\|^2) \psi(\theta, \phi) d\mathbb{S}^2 \\
&= \oint_{\mathbb{S}^2} r_i r_j \dots r_\alpha r_\beta (1) \psi(\theta, \phi) d\mathbb{S}^2 = A_{ij\dots\alpha\beta}
\end{aligned} \tag{2.10}$$

Observe, due to the symmetry conditions of Equation (2.9), there are six independent components of A_{ij} which is reduced to five components when accounting for the normalization condition of Equation (2.5). The fourth-order orientation tensor A_{ijkl} has 14 independent components, and the sixth-order orientation tensor A_{ijklmn} has 27 independent components when accounting for normalization and symmetry. Although the tensors may seem an unusual means to describe fiber orientation, they have a simple physical interpretation. For example, take an isotropic, i.e. 3-D random

orientation, state with $\psi(\theta, \phi) = \frac{1}{4\pi}$ as shown in Figure 2.2, then the second order orientation tensor is simply

$$A_{ij} = \begin{bmatrix} \frac{1}{3} & 0 & 0 \\ 0 & \frac{1}{3} & 0 \\ 0 & 0 & \frac{1}{3} \end{bmatrix} \quad (2.11)$$

When all the fibers lie along the x_1 axis as shown in Figure 2.3, the second-order orientation tensor is

$$A_{ij} = \begin{bmatrix} 1 & 0 & 0 \\ 0 & 0 & 0 \\ 0 & 0 & 0 \end{bmatrix} \quad (2.12)$$

It is often useful to reconstruct an approximate fiber orientation probability distribution function knowing only the orientation tensors (see e.g. [2, 46]) and can provide a quantitative means for assessing the effect of introducing closure approximations to represent $\psi(\theta, \phi)$ [47]. The fiber orientation distribution reconstruction introduced by Onat [?, 48] and used by Onat and Leckie [49] was initially presented for expansions up to the fourth-order and was extended by Jack and Smith [47] up to the sixth-order. Unfortunately, the means to provide expressions beyond the sixth-order were unavailable until recently where Jack and Smith [27] introduced a method, through the Laplace series of complex spherical harmonics (see e.g. [50]), to reconstruct the fiber orientation probability distribution function as

$$\psi(\theta, \phi) = \sum_{l=0}^{\infty} \sum_{m=0}^l \beta_l^m(\theta, \phi) \quad (2.13)$$

where each of the functions $\beta_l^m(\theta, \phi)$ are expressed in terms of the complex spherical harmonic functions and can be expressed as functions of the orientation tensors (see e.g. [27] for a full description). To fully describe the distribution function

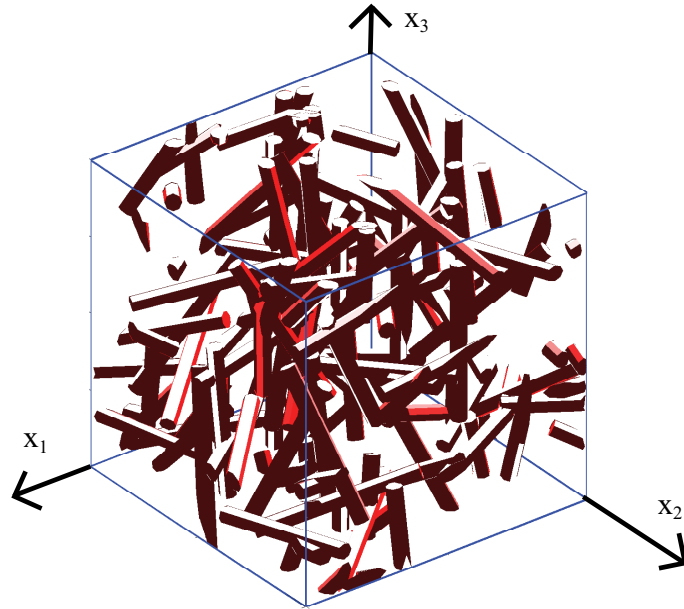


Figure 2.2: Isotropic orientation state, $\psi(\theta, \phi) = \frac{1}{4\pi}$.

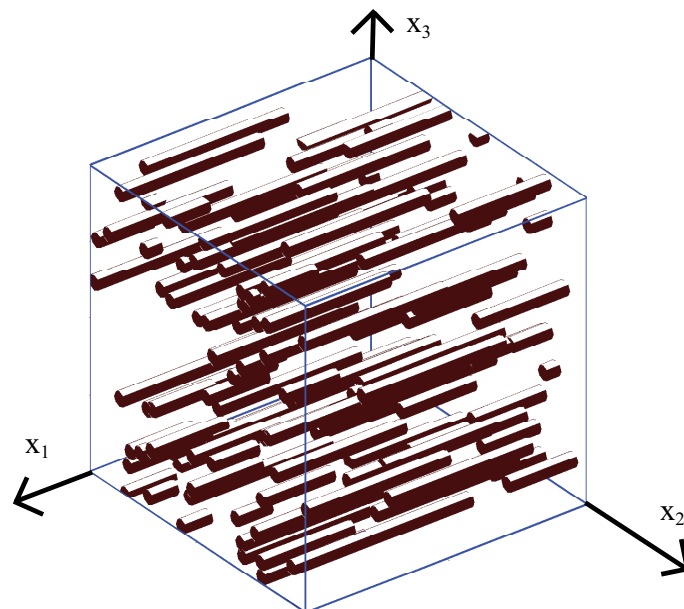


Figure 2.3: Uniaxially aligned orientation state along x_1 axis.

$\psi(\theta, \phi)$ all even-ordered orientation tensors up to infinite rank are necessary, therefore the tensor representation is always an incomplete representation of the distribution function. Conversely for many theories, the fourth-order orientation tensor provides sufficient information to predict many relevant material properties of the composite [2, 8, 25, 26, 32, 51–53], and only recently has the investigation into material stiffness representations [28] yielded a demand for orientation tensors of an order higher than fourth. It must be noted that flow simulations typically utilize solely the second- and fourth-order orientation tensors thereby neglecting any higher-order effects.

2.2 Dynamics of Fiber Orientation

The dynamics of the motion of fibers in a flow field begins with Jeffery’s model [5] where the motion of individual rigid ellipsoids in a Newtonian solvent are solved based upon first principles. The Jeffery model assumes the fluid velocity is a linear function of position in a neighborhood of the fiber and all inertia and body forces are negligible. Jeffery solved the particle motion by requiring the net forces and moments on the ellipsoid equal zero. Therefore the centroid of the particle moves with the bulk flow of the surrounding matrix. Jeffery’s solution in vector notation and index notation are, respectively, written as

$$\frac{D\mathbf{r}^h}{Dt} = \dot{\mathbf{r}}^h = -\frac{1}{2}\boldsymbol{\omega} \cdot \mathbf{r} + \frac{1}{2}\lambda(\dot{\boldsymbol{\gamma}} \cdot \mathbf{r} - \dot{\boldsymbol{\gamma}} : \mathbf{r}\mathbf{r}\mathbf{r}) \quad (2.14)$$

$$\frac{Dr_i^h}{Dt} = \dot{r}_i^h = -\frac{1}{2}\omega_{ij}r_j + \frac{1}{2}\lambda(\dot{\gamma}_{ij}r_j - \dot{\gamma}_{kl}r_k r_l r_i) \quad (2.15)$$

where $\dot{\mathbf{r}}^h$ is defined as the time derivative of the hydraulic component of rotational motion of the ellipsoid, λ depends upon the fiber aspect ratio a_r where

$\lambda = (a_r^2 - 1) / (a_r^2 + 1)$, $\dot{\gamma}_{ij}$ is the rate of deformation tensor and ω_{ij} is the vorticity tensor written as

$$\dot{\gamma}_{ij} = \frac{\partial v_j}{\partial x_i} + \frac{\partial v_i}{\partial x_j} \quad (2.16)$$

$$\omega_{ij} = \frac{\partial v_j}{\partial x_i} - \frac{\partial v_i}{\partial x_j} \quad (2.17)$$

where v_i is the i^{th} component of the velocity of the fluid. Observe in Equation (2.14) the ordinary derivative $\frac{d}{dt}$ has been replaced with the material derivative $\frac{D}{Dt}$ to recognize that the orientation may not be spatially uniform but does convect with the bulk motion of the fluid where $\frac{D}{Dt} = \frac{\partial}{\partial t} + \mathbf{v} \cdot \nabla$.

It is interesting to note that Jeffery's equation predicts that an ellipsoid in simple shearing flow will experience periodic motion labeled the Jeffery orbits. The time average of the Jeffery orbits will describe the general tendency of alignment, but in practical applications the Jeffery model is insufficient. The Jeffery model predicts that in simple shear flow after a period T , every fiber will return to its original orientation state which is not experienced by the bulk orientation in actual processes. A steady state orientation for the bulk distribution is often obtained after a short period of time with no oscillations in the distribution [1, 3, 41, 54, 55].

To employ Jeffery's model for fiber suspensions requires there be no fiber interactions. The case of non-interacting fibers is valid in the dilute regime [41, 56] defined when the inverse of the square of the aspect ratio a_r of the fiber, defined as $a_r = L/D$ where L is the fiber length and D is the fiber diameter, is much greater than the volume fraction of fibers, i.e. $V_f \ll \frac{1}{a_r^2}$. Typical fiber aspect ratios range from 10

to 20 [34], therefore for a suspension with an aspect ratio of 10 to be dilute, the fiber volume fraction would have to be much less than 1%. The semi-dilute regime is defined [41] such that $\frac{1}{a_r^2} \ll V_f \ll \frac{1}{a_r}$, therefore for an aspect ratio of 10, the semi-dilute regime would encompass a volume fraction range of $1\% \ll V_f \ll 10\%$. The concentrated regime is defined as the region where the volume fraction is greater than the inverse of the aspect ratio, i.e. $V_f > \frac{1}{a_r}$. Most typical industrial applications are in the concentrated regime, and as such the Jeffery model of Equation (2.14) is clearly not sufficient for industrial use.

Modeling the interaction between two fibers in a fluid suspension is difficult, and is the subject of continuing work. Equation (2.14) presents a location to investigate the interactions of discrete fibers, and may pose a starting point for future investigations from first principles. The present work instead investigates volume averaged effects and employs a model for fiber interactions similar to the theory of rotary Brownian motion [39, 40] where each of the ellipsoids experience small forces as they collide within the suspension causing torques upon each ellipsoid. Rotary Brownian motion has seen extensive use in the dynamics of polymeric liquids whereby individual polymer chains in a suspension are said to interact with a strong directionally dependant diffusion nature [40]. In traditional Brownian motion, if the particles are not aligned by some outside force, the orientations will eventually become random, whereas for short fiber composite flow there is no indication the fibers will reorient unless subjected to a deformation of the surrounding matrix. Assuming rigid fibers of uniform density and aspect ratio, the model of Bird [40] for rotary diffusion can be

accepted whereby the flow of a fiber distribution is given by the equation of continuity describing the conservation of mass as [40]

$$\frac{D\psi}{Dt} = -\nabla \cdot [\dot{\mathbf{r}}^h \psi(\mathbf{r}) - \nabla (D_r \psi(\mathbf{r}))] = -\nabla \cdot [\dot{\mathbf{r}}^h \psi(\mathbf{r})] + \nabla^2 [D_r \psi(\mathbf{r})] \quad (2.18)$$

where ∇ and ∇^2 represent, respectively, the gradient operator and the Laplacian operator on the surface of the unit sphere, and D_r is the rotary diffusivity to be defined later. At the present, it is sufficient to assume that D_r may be a function of (θ, ϕ) and as such cannot be brought out of the differentiation operators. When the assumptions from the Jeffery model are taken into consideration, i.e. no fiber interactions, the rotary diffusion expression D_r is set to zero. The form of Equation (2.18) has been widely accepted for rigid polymer chains and in the case of D_r being independent of direction simplifies to several of the existing theories for modeling the interaction of fibers. It is essential to advance the current understanding of fiber interaction to keep the rotary diffusivity within the Laplacian to ensure the correct directional dependance of the diffusivity is retained.

2.3 Current Models for Rotary Diffusivity in Short-Fiber Polymer Composite Processes

Kamel and Mutel [36] proposed a form for the rotary diffusivity D_r that is a function of volume fraction and independent of shear rate for a sufficiently large enough volume fraction of fibers. Their D_r was determined solely by the intensity of the interactions, but their model predicts a continually changing orientation, and independent of any applied deformation of the surrounding fluid the model predicts the fiber orientation

tends toward randomness thereby violating the physical system being modeled where the only motion of the fibers occurs during velocity changes in the surrounding fluid.

Folgar and Tucker [1] propose the rotary diffusivity be a function of both the rate of deformation tensor $\dot{\gamma}_{ij}$ and the volume fraction as

$$D_r = C_I \|\dot{\gamma}\| \quad (2.19)$$

where C_I is the empirically derived interaction coefficient assumed to be a function of volume fraction, and $\|\dot{\gamma}\|$ is the scalar magnitude of the rate-of-deformation tensor, $\|\dot{\gamma}\| = \sqrt{\frac{1}{2} \dot{\gamma}_{ij} \dot{\gamma}_{ji}}$. The Folgar and Tucker model is considered the benchmark whereby all fiber orientation analysis are based upon and has found wide acceptance within the literature [2, 3, 11, 14–16, 18, 22, 31, 42, 47, 52, 57–60]. Unlike the Kamal and Mutal model, the degree of alignment at steady state for the Folgar and Tucker model is dependent upon the strain rate. The empirically determined interaction coefficient ensures that the final orientation state is accurately captured, and has been demonstrated to be related to the volume fraction through a simple exponential function of the volume fraction of fibers [34, 41]. Although the Folgar and Tucker model is used extensively, recently there have discussions to the ability of the Folgar and Tucker model to accurately model the transient solution for the orientation of fibers [29, 33, 35, 37, 55, 61, 62].

Koch [38] presents a model for orientation diffusion resulting from the hydrodynamic fiber-fiber interactions that has seen little use in the literature. The model proposed by Koch is a function of the fourth- and sixth-order orientation tensor and has two scalable parameters that are fit to calculations of orientational diffusion in

pure extensional flows. The Koch model is presented without any derivation, and provides no experimental results to validate the model. Since the proposed model is claimed to only be valid for shearing type flows and low concentrations of fibers, it is discarded in favor of a more advanced theory.

Phan-Thien *et al.* [35] assume the rotary diffusion of the fiber distribution to be an anisotropic second-order tensor

$$\mathbf{D}_r = \mathbf{C} \|\dot{\gamma}\| \quad (2.20)$$

where bold capital letters designate a tensor. Their form assumes the diffusion follows a “white noise” random force behavior. They determine the six independent components of the tensor \mathbf{C} to the steady state solution from experimental sampling data. They relate their results back to those of the Folgar and Tucker model by assuming the interaction coefficient is related to the trace of \mathbf{C} as

$$C_I = \frac{1}{3} \text{Tr} \mathbf{C} \quad (2.21)$$

Fan *et al.* [55,61] use Equation (2.21) along with the steady state experimental results of Mondy *et al.* [63] for suspensions of fibers in Couette flow, neglecting the transient solution and demonstrate the validity of their method at steady state. Phan-Thien and coauthors [35] numerically solve the evolution equations by taking discrete fibers in a reference cell undergoing simple shear. The reference cell experiences periodic boundary conditions, i.e. a fiber leaving the reference cell from one side enters the opposite side with identical exit behavior. Phan-Thien *et al.* give all results in terms of the interaction coefficient and develop a relation between interaction coefficient

and volume fraction similar to that of Bay [34]. Unfortunately, Phan-Thien *et al.* [35] never discuss the transient results and the effect their method has upon the transient solution. Phan-Thien *et al.* conclude with the remark that the fiber interactions may not be best described by a simple diffusion process, but clearly the Folgar and Tucker model must be further investigated and improved for accurate simulations of fiber orientation.

Tucker *et al.* [29] hypothesize that the fibers experience a local strain lower than the average strain through the thickness of a part. This leads to requiring an understanding of the fluid flow regions between layers of fibers [3, 34, 54] where Tucker and co-workers hypothesize the strain is “absorbed”. Tucker *et al.* introduce a strain reduction factor, SRF , to the equation of continuity from Equation (2.18) as

$$\frac{D\psi}{Dt} = \frac{1}{SRF} (-\nabla \cdot (\dot{\mathbf{p}}^h \psi(\mathbf{p}) - \nabla (D_r \psi(\mathbf{p})))) \quad (2.22)$$

Although the results of the new model by Tucker and co-workers appears to yield adequate results in short plaque flow, the details of their model do not exist in the literature. Also, their model has the effect of retarding time to yield identical steady state results with the qualitative effect of tracing the same orientation path in space.

CHAPTER 3

INCORPORATION OF DIRECTIONALLY DEPENDANT DIFFUSION

Phan-Thien *et al.* [35] and Tucker *et al.* [29] both concur that there is a need to improve the widely used Folgar-Tucker model to correctly represent the transient behavior of the fiber orientation distribution function, not just the steady state orientation. Qualitatively, the use of the Folgar and Tucker model predicts the fiber orientation 2 to 3 times faster than as seen experimentally [29].

As discussed in Folgar and Tucker [1] the form for their diffusion term $D_r = C_I ||\dot{\gamma}||$ was based upon experimental observations for fiber behavior in concentrated suspensions. They observed that an individual fiber follows the Jeffery orbits discussed in Equation (2.14) for short periods of time, but will with apparent randomness quickly reorient to another angle and resumes following the trend of Equation (2.14) again. Clearly these reorientations are caused by fiber interactions tending to randomize the orientation. Folgar and Tucker speculated that their diffusion term could be constructed to have a directional bias to account for the differences between random and aligned suspension behavior, but chose not to include such effects.

3.1 General Form for Directionally Dependant Diffusion

To investigate the effects the distribution of fibers has upon fiber interactions, the role of various factors must be considered. Clearly the diffusion must be a function

of the number of collisions. In other words, if the fluid experiences no deformation or motion there will be no tendency for fibers to move relative to their neighbor since external forces are neglected as are true Brownian effects. Ergo, the diffusion must depend upon the rate-of-deformation tensor $\dot{\boldsymbol{\gamma}}$ given in Equation (2.16) and may be used to describe the tendency of a given particle to move relative to its neighbor. The diffusion must also be a function of volume fraction V_f , i.e. with an increased number of fibers there will be an increase in the number of collisions. Orientation effects will be considered through the fiber orientation probability distribution function $\psi(\theta, \phi)$. Consider the two dimensional examples presented in Figures 3.1 and 3.2 for the single fiber, colored black, placed within an isotropic and nearly aligned two dimensional distribution. The fiber in Figure 3.1 will experience no preferred orientation changes other than those from the bulk motion of the surrounding fluid. Statistically fibers placed within the distribution of fibers given in Figure 3.1 will tend toward a random orientation at a rate based upon the number of collisions. Conversely, the fiber in Figure 3.2 will have a tendency to align parallel with the aligned distribution at a rate related to the number of collisions. Therefore there will be a strong directional dependance upon the preferred orientation due to the fiber-fiber collisions. To prevent any loss of generality throughout the derivations, unless otherwise noted, the diffusion is assumed to be a general function of the fiber orientation probability distribution function $\psi(\theta, \phi)$, direction \mathbf{r} , the fiber aspect ratio through the parameter λ , fiber volume fraction V_f and rate-of-deformation $\dot{\boldsymbol{\gamma}}$ as

$$D_r = D_r(\psi(\theta, \phi), \mathbf{r}, V_f, \dot{\boldsymbol{\gamma}}) \quad (3.1)$$

where the diffusion is assumed to be as continuous a function as necessary throughout the derivation.

3.2 Orientation Tensor Evolution

Computer simulations that evaluate $\psi(\theta, \phi, t)$, where t is time, for simple flows may require several weeks to several months of computational resources to reach steady state and as such are impractical to be considered for industrial simulations. Alternatively, the orientation tensor approach of Advani and Tucker [2] represents the distribution function of fibres in a concise form thereby alleviating the overwhelming computational burden. Industrial simulations to model the fiber orientation state employ the orientation tensor approach of Advani and Tucker, and as such their approach will be utilized throughout the remainder of the text.

The following section will develop the equation of motion for the second-order orientation tensor with the basic assumptions given in Equation (3.1) for the rotary diffusion. The derivation takes place in spherical coordinates and is undertaken by pre-multiplying the equation of continuity from Equation (2.18) with the test function $\mathbf{B} = \mathbf{pp}$ and integrating over \mathbb{S}^2 . This choice of test function will produce the equation of motion for the second-order orientation tensor $A_{\alpha\beta}$ given below as

$$\begin{aligned} \frac{DA_{\alpha\beta}}{Dt} &= -\frac{1}{2}\omega_{\alpha j}A_{j\beta} + \frac{1}{2}A_{\alpha j}\omega_{j\beta} + \frac{1}{2}\lambda(\dot{\gamma}_{\alpha j}A_{j\beta} + A_{\alpha j}\dot{\gamma}_{j\beta} - 2\dot{\gamma}_{ij}A_{ij\alpha\beta}) \\ &\quad + \oint_{\mathbb{S}^2} D_r\psi(2\delta_{\alpha\beta} - 6r_\alpha r_\beta) d\mathbb{S} \end{aligned} \quad (3.2)$$

Notice the equation of motion for $A_{\alpha\beta}$ is a function of the fourth-order orientation tensor $A_{ij\alpha\beta}$. A similar derivation as given below can be undertaken for the equation

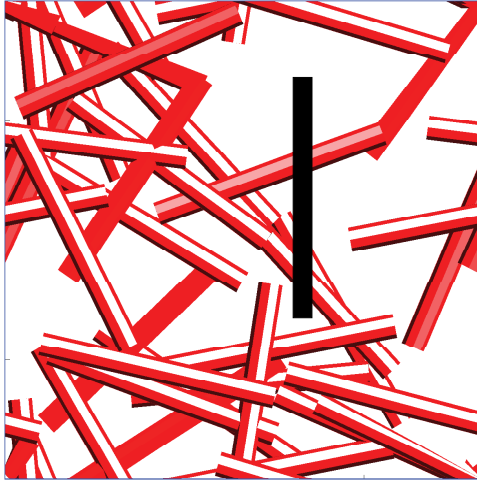


Figure 3.1: Single fiber within an isotropic 2-D fiber distribution.

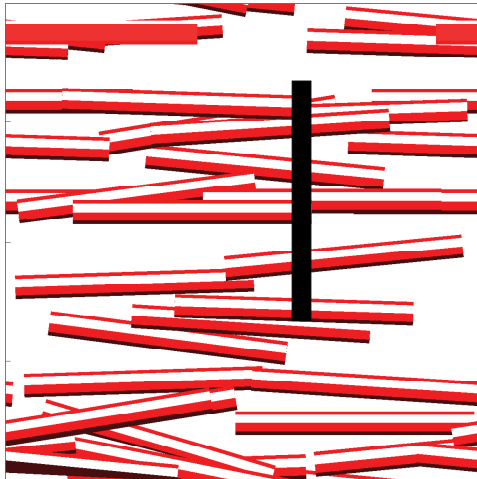


Figure 3.2: Single fiber within a highly aligned 2-D fiber distribution.

of motion for the fourth-order orientation tensor and will yield a function that requires the sixth-order orientation tensor A_{ijklmn} . The equation of motion for $A_{\alpha\beta}$ is presented in the following section because of the widespread industrial use of the second-order orientation tensor in production simulations.

3.2.1 Spherical Coordinate Representation

The derivation is undertaken on the surface of the unit sphere with the coordinate system taken to be that given in Figure 2.1. Therefore an understanding of spherical coordinates and the derivatives of the spherical unit vectors is essential. The spherical coordinate unit vectors \mathbf{r} , $\boldsymbol{\phi}$, and $\boldsymbol{\theta}$ are simply [64]

$$\mathbf{r} = \begin{Bmatrix} \sin\theta \cos\phi \\ \sin\theta \sin\phi \\ \cos\theta \end{Bmatrix} \quad \boldsymbol{\phi} = \begin{Bmatrix} -\sin\phi \\ \cos\phi \\ 0 \end{Bmatrix} \quad \boldsymbol{\theta} = \begin{Bmatrix} \cos\phi \cos\theta \\ \sin\phi \cos\theta \\ -\sin\theta \end{Bmatrix} \quad (3.3)$$

where the bold font on a lower case letter designates a vector belonging to \mathbb{R}^3 , and a bold capital letter will be used for a tensor. Observe, the spherical coordinate \mathbf{r} is identical to the definition of the unit vector \mathbf{r} aligned along the fiber axis given in Equation (2.1) and shown in Figure 2.1. Unlike Cartesian coordinates, derivatives of the coordinate unit vectors in spherical coordinates are not identically zero. The derivatives of the unit coordinate vectors are [64]

$$\begin{aligned} \frac{\partial \mathbf{r}}{\partial r} &= \mathbf{0} & \frac{\partial \mathbf{r}}{\partial \phi} &= \sin\theta \boldsymbol{\phi} & \frac{\partial \mathbf{r}}{\partial \theta} &= \boldsymbol{\theta} \\ \frac{\partial \boldsymbol{\phi}}{\partial r} &= \mathbf{0} & \frac{\partial \boldsymbol{\phi}}{\partial \phi} &= -\cos\theta \boldsymbol{\theta} - \sin\theta \mathbf{r} & \frac{\partial \boldsymbol{\phi}}{\partial \theta} &= \mathbf{0} \\ \frac{\partial \boldsymbol{\theta}}{\partial r} &= \mathbf{0} & \frac{\partial \boldsymbol{\theta}}{\partial \phi} &= \cos\theta \boldsymbol{\phi} & \frac{\partial \boldsymbol{\theta}}{\partial \theta} &= -\mathbf{r} \end{aligned} \quad (3.4)$$

Additionally, it will be useful to recognize that the Kronecker Delta δ_{ij} is written as

$$\delta_{ij} = r_i r_j + \theta_i \theta_j + \phi_i \phi_j \quad (3.5)$$

where r_i , θ_i and ϕ_i are the i^{th} components of the unit vectors \mathbf{r} , $\boldsymbol{\theta}$ and $\boldsymbol{\phi}$ respectively.

The i^{th} component of the gradient on the surface of the unit sphere where $r = 1$ is given as

$$\nabla_i = \theta_i \frac{\partial}{\partial \theta} + \phi_i \frac{1}{\sin \theta} \frac{\partial}{\partial \phi} \quad (3.6)$$

and the Laplacian in spherical coordinates on the surface of the unit sphere is simply

$$\nabla^2 = \frac{1}{\sin^2 \theta} \frac{\partial^2}{\partial \phi^2} + \frac{\cos \theta}{\sin \theta} \frac{\partial}{\partial \theta} + \frac{\partial^2}{\partial \theta^2} \quad (3.7)$$

3.2.2 Equation of Change for $\mathbf{B}(\mathbf{r}) = \mathbf{r}\mathbf{r}$

As discussed in the introduction, most industrial applications are interested in the second- and fourth-order orientation tensor to obtain material properties. Additionally, since there exist many methods to approximate the fourth-order orientation tensor once the second order orientation tensor is known (see e.g. [7–18]), the industrially relevant equation of change is that of the second-order orientation tensor where the tensor $\mathbf{B}(\mathbf{r})$ will be given in component form as $B_{\alpha\beta} = r_\alpha r_\beta$ for $\alpha, \beta \in \{1, 2, 3\}$. Observe $\oint_{\mathbb{S}^2} \psi(\theta, \phi) \mathbf{B}(\mathbf{r}) d\mathbb{S} = \oint_{\mathbb{S}^2} \psi(\theta, \phi) \mathbf{r}\mathbf{r} d\mathbb{S}$ is the second-order orientation tensor defined in Equation (2.8). To derive the equation of change associated with the tensor $\mathbf{B}(\mathbf{r})$, post-multiply Equation (2.18), the equation of continuity with rotary diffusion, with the α, β component of the test function $\mathbf{B}(\mathbf{r})$, where the integral over all space is expressed as

$$\oint_{\mathbb{S}^2} \frac{D\psi}{Dt} B_{\alpha\beta} d\mathbb{S} = - \oint_{\mathbb{S}^2} \nabla \cdot (\dot{\mathbf{r}}^h \psi - \nabla (D_r \psi)) B_{\alpha\beta} d\mathbb{S} \quad (3.8)$$

where it is assumed that $B_{\alpha\beta}$, ψ and D_r each depend upon \mathbf{r} . Observe, the left hand side of the equation is the desired form for the equation of motion for the second-order orientation tensor $A_{\alpha\beta}$ which is seen as

$$\oint_{\mathbb{S}^2} \frac{D\psi}{Dt} B_{\alpha\beta} d\mathbb{S} = \frac{D}{Dt} \oint_{\mathbb{S}^2} \psi B_{\alpha\beta} d\mathbb{S} = \frac{D}{Dt} \oint_{\mathbb{S}^2} \psi r_\alpha r_\beta d\mathbb{S} = \frac{DA_{\alpha\beta}}{Dt} \quad (3.9)$$

where the material derivative $\frac{D}{Dt}$ can be brought outside the integration since the integration over the unit sphere is independent of time.

Using the chain rule to expand the right hand side of Equation (3.8) one obtains

$$\begin{aligned} & \oint_{\mathbb{S}^2} \nabla \cdot (\dot{\mathbf{r}}^h \psi - \nabla (D_r \psi)) B_{\alpha\beta} d\mathbb{S} = \\ & \oint_{\mathbb{S}^2} \nabla \cdot ((\dot{\mathbf{r}}^h \psi - \nabla (D_r \psi)) B_{\alpha\beta}) d\mathbb{S} - \oint_{\mathbb{S}^2} (\dot{\mathbf{r}}^h \psi - \nabla (D_r \psi)) \cdot \nabla (B_{\alpha\beta}) d\mathbb{S} \end{aligned} \quad (3.10)$$

From Evans [65], the divergence of a continuous function F on a sphere is simply $\oint_{\mathbb{S}^2} \nabla \cdot F d\mathbb{S} = 0$, therefore the first term on the right hand side of Equation (3.10) is zero assuming $(\dot{\mathbf{r}}^h \psi - \nabla (D_r \psi)) B_{\alpha\beta}$ is a continuous function. Since it is assumed that the distribution function $\psi(\theta, \phi)$ is continuous with respect to \mathbf{r} as is the rate of deformation tensor used to form $\dot{\mathbf{r}}^h$, then the gradient of D_r must also be continuous within the unit sphere. Ergo, D_r must be first-order differentiable within and on the unit sphere.

Rewriting Equation (3.8) with Equation (3.10) and expanding the integration recognizing both integrands are integrable, the equation of motion for the second-order orientation tensor is simply the sum of two components

$$\frac{DA_{\alpha\beta}}{Dt} = \oint_{\mathbb{S}^2} \dot{\mathbf{r}}^h \psi \cdot \nabla (B_{\alpha\beta}) d\mathbb{S} - \oint_{\mathbb{S}^2} \nabla (D_r \psi) \cdot \nabla (B_{\alpha\beta}) d\mathbb{S} \quad (3.11)$$

The first component represents the change in the equation of motion due to hydrodynamic forces as given by Jeffery's equation, and the second component represents effects due to rotary diffusion.

3.2.2.1 Equation of Change: Jeffery's Equation

Observe the first term on the right hand side of Equation (3.11) is only dependant upon Jeffery's equation and the choice of the test function. Using $B_{\alpha\beta} = r_\alpha r_\beta$, the integration can be expressed as

$$\begin{aligned} \oint_{\mathbb{S}^2} \dot{\mathbf{r}}^h \psi \cdot \nabla (r_\alpha r_\beta) d\mathbb{S} &= \oint_{\mathbb{S}^2} \dot{r}_i^h \psi \nabla_i (r_\alpha r_\beta) d\mathbb{S} \\ &= \oint_{\mathbb{S}^2} \dot{r}_i^h \psi \left(\theta_i \frac{\partial}{\partial \theta} (r_\alpha r_\beta) + \phi_i \frac{1}{\sin \theta} \frac{\partial}{\partial \phi} (r_\alpha r_\beta) \right) d\mathbb{S} \end{aligned} \quad (3.12)$$

The derivatives are computed using the chain rule and Equation (3.4) to compute the derivatives of the unit vectors in spherical coordinates. Then Equation (3.12) is rewritten as

$$\oint_{\mathbb{S}^2} \dot{\mathbf{r}}^h \psi \cdot \nabla (r_\alpha r_\beta) d\mathbb{S} = \oint_{\mathbb{S}^2} \dot{r}_i^h \psi (\theta_i (\theta_\alpha r_\beta + r_\alpha \theta_\beta) + \phi_i (\phi_\alpha r_\beta + r_\alpha \phi_\beta)) d\mathbb{S} \quad (3.13)$$

Inserting Jeffery's equation for the motion of a fiber from Equation (2.14) for \dot{r}_i^h into the above equation one obtains

$$\begin{aligned} &\oint_{\mathbb{S}^2} \dot{\mathbf{r}}^h \psi \cdot \nabla (r_\alpha r_\beta) d\mathbb{S} \\ &= \frac{1}{2} \oint_{\mathbb{S}^2} \psi (-\omega_{ij} r_j + \lambda (\dot{\gamma}_{ij} r_j - \dot{\gamma}_{kl} r_k r_l r_i)) (\theta_i (\theta_\alpha r_\beta + r_\alpha \theta_\beta) + \phi_i (\phi_\alpha r_\beta + r_\alpha \phi_\beta)) d\mathbb{S} \\ &= \frac{1}{2} \oint_{\mathbb{S}^2} \psi [-\omega_{ij} (r_j \theta_i \theta_\alpha r_\beta + r_j \phi_i \phi_\alpha r_\beta + r_j \theta_i \theta_\beta r_\alpha + r_j \phi_i \phi_\beta r_\alpha) \\ &\quad + \lambda \dot{\gamma}_{ij} (r_j \theta_i \theta_\alpha r_\beta + r_j \phi_i \phi_\alpha r_\beta + r_j \theta_i \theta_\beta r_\alpha + r_j \phi_i \phi_\beta r_\alpha) \\ &\quad - \lambda \dot{\gamma}_{kl} r_k r_l (r_i \theta_i \theta_\alpha r_\beta + r_i \phi_i \phi_\alpha r_\beta + r_i \theta_i \theta_\beta r_\alpha + r_i \phi_i \phi_\beta r_\alpha)] d\mathbb{S} \end{aligned} \quad (3.14)$$

Rewriting the above with Equation (3.5) to remove the $\boldsymbol{\theta}$ and $\boldsymbol{\phi}$ vectors

$$\begin{aligned}
& \oint_{\mathbb{S}^2} \dot{\mathbf{r}}^h \psi \cdot \nabla (r_\alpha r_\beta) \, d\mathbb{S} \\
&= \frac{1}{2} \oint_{\mathbb{S}^2} \psi [-\omega_{ij} (r_j (\theta_i \theta_\alpha + \phi_i \phi_\alpha) r_\beta + r_j (\theta_i \theta_\beta + \phi_i \phi_\beta) r_\alpha) \\
&\quad + \lambda \dot{\gamma}_{ij} (r_j (\theta_i \theta_\alpha + \phi_i \phi_\alpha) r_\beta + r_j (\theta_i \theta_\beta + \phi_i \phi_\beta) r_\alpha) \\
&\quad - \lambda \dot{\gamma}_{kl} r_k r_l (r_i (\theta_i \theta_\alpha + \phi_i \phi_\alpha) r_\beta + r_i (\theta_i \theta_\beta + \phi_i \phi_\beta) r_\alpha)] \, d\mathbb{S} \\
&= \frac{1}{2} \oint_{\mathbb{S}^2} \psi [-\omega_{ij} (r_j r_\beta \delta_{i\alpha} - r_j r_\beta r_i r_\alpha + r_j r_\alpha \delta_{i\beta} - r_j r_\alpha r_i r_\beta) \\
&\quad + \lambda \dot{\gamma}_{ij} (r_j r_\beta \delta_{i\alpha} - r_j r_\beta r_i r_\alpha + r_j r_\alpha \delta_{i\beta} - r_j r_\alpha r_i r_\beta) \\
&\quad - \lambda \dot{\gamma}_{kl} r_k r_l (r_i r_\beta \delta_{i\alpha} - r_i r_\beta r_i r_\alpha + r_i r_\alpha \delta_{i\beta} - r_i r_\alpha r_i r_\beta)] \, d\mathbb{S} \quad (3.15)
\end{aligned}$$

Recall from Equation (2.16), that $\omega_{ij} = -\omega_{ji}$, $\dot{\gamma}_{ij} = \dot{\gamma}_{ji}$, and $r_i r_i = 1$, then the above is simplified as

$$\begin{aligned}
& \oint_{\mathbb{S}^2} \dot{\mathbf{r}}^h \psi \cdot \nabla (r_\alpha r_\beta) \, d\mathbb{S} \\
&= \frac{1}{2} \oint_{\mathbb{S}^2} \psi [-\omega_{\alpha j} r_j r_\beta + \omega_{j\beta} r_j r_\alpha + (\omega_{ij} r_i r_j r_\alpha r_\beta - \omega_{ji} r_j r_i r_\alpha r_\beta) \\
&\quad + \lambda \dot{\gamma}_{\alpha j} r_j r_\beta + \lambda \dot{\gamma}_{j\beta} r_j r_\alpha - \lambda (\dot{\gamma}_{ij} r_i r_j r_\alpha r_\beta + \dot{\gamma}_{ji} r_j r_i r_\alpha r_\beta) \\
&\quad - \frac{1}{2} \lambda \dot{\gamma}_{kl} r_k r_l (r_\alpha r_\beta - r_\beta r_\alpha + r_\beta r_\alpha - r_\alpha r_\beta)] \, d\mathbb{S} \\
&= \frac{1}{2} \oint_{\mathbb{S}^2} \psi [-\omega_{\alpha j} r_j r_\beta + \omega_{j\beta} r_j r_\alpha + (\omega_{ij} r_i r_j r_\alpha r_\beta - \omega_{ij} r_i r_j r_\alpha r_\beta) \\
&\quad + \lambda \dot{\gamma}_{\alpha j} r_j r_\beta + \lambda \dot{\gamma}_{j\beta} r_j r_\alpha - \lambda (\dot{\gamma}_{ij} r_i r_j r_\alpha r_\beta + \dot{\gamma}_{ij} r_i r_j r_\alpha r_\beta)] \, d\mathbb{S} \\
&= \frac{1}{2} \oint_{\mathbb{S}^2} \psi [-\omega_{\alpha j} r_j r_\beta + \omega_{j\beta} r_j r_\alpha \\
&\quad + \lambda \dot{\gamma}_{\alpha j} r_j r_\beta + \lambda \dot{\gamma}_{j\beta} r_j r_\alpha - 2\lambda (\dot{\gamma}_{ij} r_i r_j r_\alpha r_\beta)] \, d\mathbb{S} \quad (3.16)
\end{aligned}$$

Where the last step used the fact that i and j are dummy indices and can be switched interchangeably therefore $\omega_{ji}r_jr_ir_\alpha r_\beta = \omega_{ij}r_ir_jr_\alpha r_\beta$. Recognizing the rate-of-deformation tensor and vorticity tensor are assumed constant over the area of integration, Equation (3.16) can be written in tensor form yielding the equation of change for the second-order orientation tensor from the hydrodynamic effects from Jeffery's model as

$$\begin{aligned}
& \oint_{\mathbb{S}^2} \dot{\mathbf{r}}^h \psi \cdot \nabla (r_\alpha r_\beta) \, d\mathbb{S} \\
&= -\frac{1}{2} \omega_{\alpha j} \oint_{\mathbb{S}^2} \psi r_j r_\beta \, d\mathbb{S} + \frac{1}{2} \oint_{\mathbb{S}^2} \psi r_\alpha r_j \, d\mathbb{S} \omega_{j\beta} \\
&\quad + \frac{1}{2} \lambda \left(\dot{\gamma}_{\alpha j} \oint_{\mathbb{S}^2} \psi r_j r_\beta \, d\mathbb{S} + \oint_{\mathbb{S}^2} \psi r_\alpha r_j \, d\mathbb{S} \dot{\gamma}_{j\beta} - 2\dot{\gamma}_{ij} \oint_{\mathbb{S}^2} \psi r_i r_j r_\alpha r_\beta \, d\mathbb{S} \right) \\
&= -\frac{1}{2} \omega_{\alpha j} A_{j\beta} + \frac{1}{2} A_{\alpha j} \omega_{j\beta} + \frac{1}{2} \lambda (\dot{\gamma}_{\alpha j} A_{j\beta} + A_{\alpha j} \dot{\gamma}_{j\beta} - 2\dot{\gamma}_{ij} A_{ij\alpha\beta}) \quad (3.17)
\end{aligned}$$

Observe that the final term in Equation (3.17) is the fourth-order orientation tensor $A_{ij\alpha\beta}$. A similar derivation can be used to derive the equation of change for the fourth-order orientation tensor whereby the sixth-order orientation tensor will appear. Therein lies the classical closure dilemma, whereby the higher order orientation tensor must be approximated as some function of the lower order orientation tensor. As previously discussed there are many closures in the literature for the fourth-order orientation tensor and the sixth-order orientation tensor for short fiber polymer composites. This problem is not constrained to polymer composite flow, but also appears in crystalline polymer flow [66], crack fabric tensors [67], and turbulent flow [68].

3.2.2.2 Equation of Change: Directionally Dependant Diffusion

The integration associated with the rotary diffusion on the right hand side of Equation (3.11) for the equation of flow of the orientation tensor can be written using the chain rule for gradients as

$$- \oint_{\mathbb{S}^2} \nabla (D_r \psi) \cdot \nabla (B_{\alpha\beta}) \, d\mathbb{S} = \oint_{\mathbb{S}^2} D_r \psi \nabla^2 (B_{\alpha\beta}) \, d\mathbb{S} - \oint_{\mathbb{S}^2} \nabla \cdot (D_r \psi \nabla (B_{\alpha\beta})) \, d\mathbb{S} \quad (3.18)$$

As discussed in previously, the integral of the divergence of a continuous function over a closed surface is zero. Therefore since it is assumed that the rotary diffusion D_r is first-order continuous, the second term on the right hand side of the previous equation is zero. The definition of the Laplacian in spherical coordinates from Equation (3.7) is used solve $\nabla^2 B_{\alpha\beta}$ as

$$\begin{aligned} \nabla^2 (B_{\alpha\beta}) &= \nabla^2 (r_\alpha r_\beta) \\ &= \frac{1}{\sin^2 \theta} \frac{\partial^2}{\partial \phi^2} (r_\alpha r_\beta) + \frac{\cos \theta}{\sin \theta} \frac{\partial}{\partial \theta} (r_\alpha r_\beta) + \frac{\partial^2}{\partial \theta^2} (r_\alpha r_\beta) \\ &= \frac{1}{\sin^2 \theta} \frac{\partial}{\partial \phi} (\sin \theta \phi_\alpha r_\beta + \sin \theta r_\alpha \phi_\beta) + \frac{\cos \theta}{\sin \theta} (\theta_\alpha r_\beta + r_\alpha \theta_\beta) + \frac{\partial}{\partial \theta} (\theta_\alpha r_\beta + r_\alpha \theta_\beta) \\ &= \left(-\frac{\cos \theta}{\sin \theta} \theta_\alpha r_\beta - r_\alpha r_\beta + \phi_\alpha \phi_\beta + \phi_\alpha \phi_\beta - \frac{\cos \theta}{\sin \theta} r_\alpha \theta_\beta - r_\alpha r_\beta \right) \\ &\quad + \frac{\cos \theta}{\sin \theta} (\theta_\alpha r_\beta + r_\alpha \theta_\beta) + (-r_\alpha r_\beta + \theta_\alpha \theta_\beta + \theta_\alpha \theta_\beta - r_\alpha r_\beta) \\ &= \frac{\cos \theta}{\sin \theta} (\theta_\alpha r_\beta + r_\alpha \theta_\beta) - 2r_\alpha r_\beta + 2\phi_\alpha \phi_\beta - \frac{\cos \theta}{\sin \theta} (\theta_\alpha r_\beta + r_\alpha \theta_\beta) \\ &\quad - 2r_\alpha r_\beta + 2\theta_\alpha \theta_\beta \end{aligned} \quad (3.19)$$

Simplifying the expression by recognizing $\delta_{ij} = r_i r_j + \phi_i \phi_j + \theta_i \theta_j$ from Equation (3.5)

$$\begin{aligned} \nabla^2 (B_{\alpha\beta}) &= -4r_\alpha r_\beta + 2\phi_\alpha \phi_\beta + 2\theta_\alpha \theta_\beta \\ &= -4r_\alpha r_\beta + 2\delta_{\alpha\beta} - 2r_\alpha r_\beta = 2\delta_{\alpha\beta} - 6r_\alpha r_\beta \end{aligned} \quad (3.20)$$

Therefore, the second term on the right hand side of Equation (3.11) simplifies to

$$-\oint_{\mathbb{S}^2} \nabla (D_r \psi) \cdot \nabla (B_{\alpha\beta}) \, d\mathbb{S} = \oint_{\mathbb{S}^2} D_r \psi (2\delta_{\alpha\beta} - 6r_\alpha r_\beta) \, d\mathbb{S} \quad (3.21)$$

The equation of motion for the second-order orientation tensor presented in Equation (3.2) is readily obtained by combining Equations (3.17) and (3.21) with Equation (3.11).

CHAPTER 4

DIRECTIONALLY DEPENDANT DIFFUSION MODELS

This work presents two models to incorporate fiber interactions through the diffusion of the fiber probability orientation distribution function. The two forms serve to model the qualitative behavior of fiber orientation in semi-dilute and concentrated suspensions. It is recognized these models satisfy the qualitative requirements outlined in the introduction, but there is still much work to be done to develop an accurate mathematical model of the physical phenomena that drive fiber orientation kinematics in a densely packed fiber melt. The preliminary model discussed in Jack [69] is a simple first-order approximation to demonstrate the qualitative effects desired in the ideal model. This model is presented because of the relative ease of implementation in current industrial simulations for modeling fiber interaction effects. The first model provides scalable parameters that serve to draw out the time to align the flows, but produces non-physical numerical results for large values of the scalable parameter. alternatively, the second, advanced, model has all the desired effects expressed in the introduction. The scalable parameters for the second model allow easy adjustments at the rate at which fibers align while attaining nearly the same steady state results as observed in the laboratory environment. These scalable parameters serve to elongate the transient solution by as much as three time scales, while remaining within physical orientation states for all flows investigated. The second-model provides the

desired results at the cost of knowing the orientation tensors up to the tenth-order for the second-order orientation tensor evolutions.

4.1 Preliminary Model for First-Order Directionally Dependant Diffusion

The preliminary model discussed simply approximates the directionally dependant diffusion D_r as a linear combination between the first moment of a single fiber and the trace of the second-moment of the fiber's orientation with the second-order orientation tensor, A_{ij} as

$$D_r = \|\dot{\gamma}\| (D_1 + D_2 A_{kl} r_k r_l) \quad (4.1)$$

where $\|\dot{\gamma}\| = \sqrt{\frac{1}{2} \dot{\gamma}_{ij} \dot{\gamma}_{ji}}$ is the scalar magnitude of the strain rate tensor. Observe this form satisfies the criteria outlined in Equation (3.1) for an acceptable model for directional diffusion. The model incorporates the rate of collisions through the scalar rate of deformation, the directionality of the distribution through the second-order orientation tensor, and the volume fraction can be incorporated into the scalar parameters D_1 and D_2 . In the limiting case with $D_2 = 0$ and $D_1 = C_I$, where C_I is the fiber interaction coefficient from the Folgar and Tucker model [1], Equation (3.2) can be simplified with D_r from Equation (4.1) to the orientation tensor representation of the Folgar and Tucker model outlined by Advani [6].

Observe that the coefficients D_1 and D_2 , when positive, will tend to cause the fibers to deviate from perfect alignment. The larger D_1 is set, the more the steady state orientation will tend toward randomly oriented. For negative values of D_2 the

orientation will tend to become aligned at steady state, and as such D_2 will tend to offset the effects of D_1 . The parameter D_2 serves a second purpose, the larger in magnitude (i.e. more negative) D_2 is selected the longer it will take for an initially isotropic fiber orientation to reach steady state.

4.1.1 Graphical Description for First-Order Model

To serve as visual reference, several examples are presented to demonstrate the first-order directionally dependant diffusion model, where each example is normalized with $\|\dot{\gamma}\| = 1$ and $D_1 = -D_2 = 1$. The first example is that of an isotropic fiber orientation probability distribution, $\psi(\theta, \phi) = \frac{1}{4\pi}$. Observe, this distribution will yield the same second-order orientation tensor given in Equation (2.11) where $A_{11} = A_{22} = A_{33} = \frac{1}{3}$ and $A_{ij} = 0 \forall i \neq j$. As evidenced in Figure 4.1, the rotary diffusion is a constant value implying that any fiber placed within a matrix with an isotropic fiber distribution will not have a preferred orientation similar to the discussion of Figure 3.1 from the preceding chapter.

Conversely, take the distribution of fibers aligned along the x_1 axis as in Figure 2.3 where $A_{11} = 1$, $A_{22} = A_{33} = 0$ and $A_{ij} = 0 \forall i \neq j$. The function $D_r(\theta, \phi)$ for this unidirectional alignment state is given in Figure 4.2. Note how a fiber aligned along the x_1 axis, given by $(\theta, \phi) = (\frac{\pi}{2}, 0)$, has a value of zero, satisfying the requirement discussed in Figure 3.2 that a fiber placed parallel to a unidirectional set of fibers will not have a propensity to move from alignment with the unidirectional fibers. On the other hand, a fiber perpendicular to the unidirectional distribution, say

$(\theta, \phi) = (\pi, 0)$ will experience significant amounts of diffusion causing the fiber to rotate from perpendicular with the surrounding fibers to align along the unidirectional fiber alignment.

The final example is for a fiber distribution randomly aligned in the $x_1 - x_2$ plane with no fibers having any orientation in the x_3 direction. This planar, random distribution may be found in thin molds where the part thickness is on the order of the fiber length. The directional diffusion function from the preliminary model is shown in Figure 4.3, and as expected, a fiber placed perpendicular to the plane in which the surrounding fibers lie, i.e. $\theta = 0$ or $\theta = \pi$, will experience a large degree of diffusion tending to align the fiber in the $x_1 - x_2$ plane, but experiencing no preferred orientation in the $x_1 - x_2$ plane as shown by the flat valley along $\theta = \frac{\pi}{2}$.

4.1.2 Orientation Tensor Evolution Formulation and Results

The second-order orientation tensor evolution of Equation (3.2) with general rotary diffusion $D_r(\theta, \phi)$ is approximated by the first-order model for directionally dependant diffusion of Equation (4.1) as

$$\begin{aligned}
\frac{DA_{\alpha\beta}}{Dt} &= -\frac{1}{2}\omega_{\alpha j}A_{j\beta} + \frac{1}{2}A_{\alpha j}\omega_{j\beta} + \frac{1}{2}\lambda(\dot{\gamma}_{\alpha j}A_{j\beta} + A_{\alpha j}\dot{\gamma}_{j\beta} - 2\dot{\gamma}_{ij}A_{ij\alpha\beta}) \\
&\quad + \oint_{\mathbb{S}^2} \|\dot{\gamma}\| (D_1 + D_2 a_{kl} r_k r_l) \psi (2\delta_{\alpha\beta} - 6r_\alpha r_\beta) d\mathbb{S} \\
&= -\frac{1}{2}\omega_{\alpha j}A_{j\beta} + \frac{1}{2}A_{\alpha j}\omega_{j\beta} + \frac{1}{2}\lambda(\dot{\gamma}_{\alpha j}A_{j\beta} + A_{\alpha j}\dot{\gamma}_{j\beta} - 2\dot{\gamma}_{ij}A_{ij\alpha\beta}) \\
&\quad + \oint_{\mathbb{S}^2} \|\dot{\gamma}\| D_1 \psi (2\delta_{\alpha\beta} - 6r_\alpha r_\beta) d\mathbb{S} + \oint_{\mathbb{S}^2} \|\dot{\gamma}\| D_2 a_{kl} r_k r_l \psi (2\delta_{\alpha\beta} - 6r_\alpha r_\beta) d\mathbb{S} \quad (4.2)
\end{aligned}$$

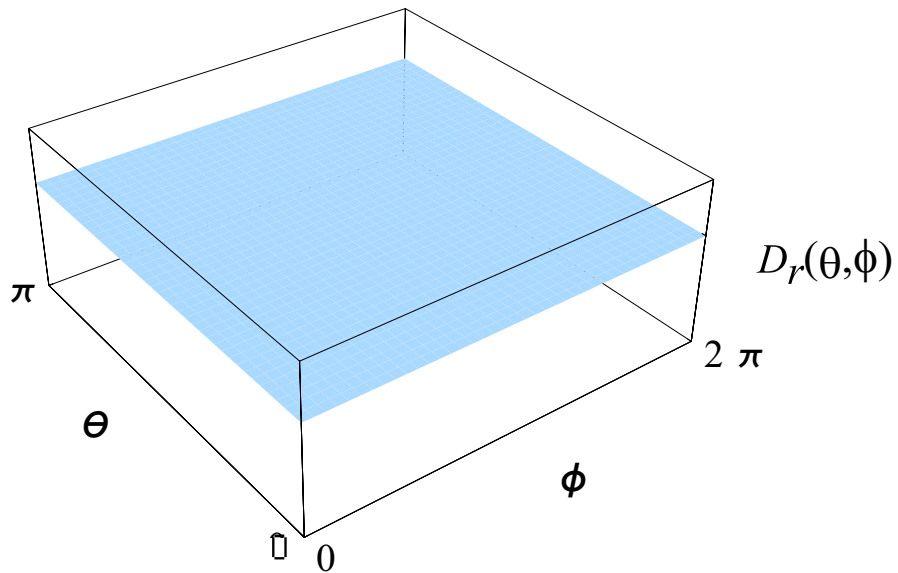


Figure 4.1: First-order directionally dependant diffusion, $D_r(\theta, \phi)$, for isotropic fiber orientation state, $\psi(\theta, \phi) = \frac{1}{4\pi}$ (normalized with $\|\dot{\gamma}\| = 1$).

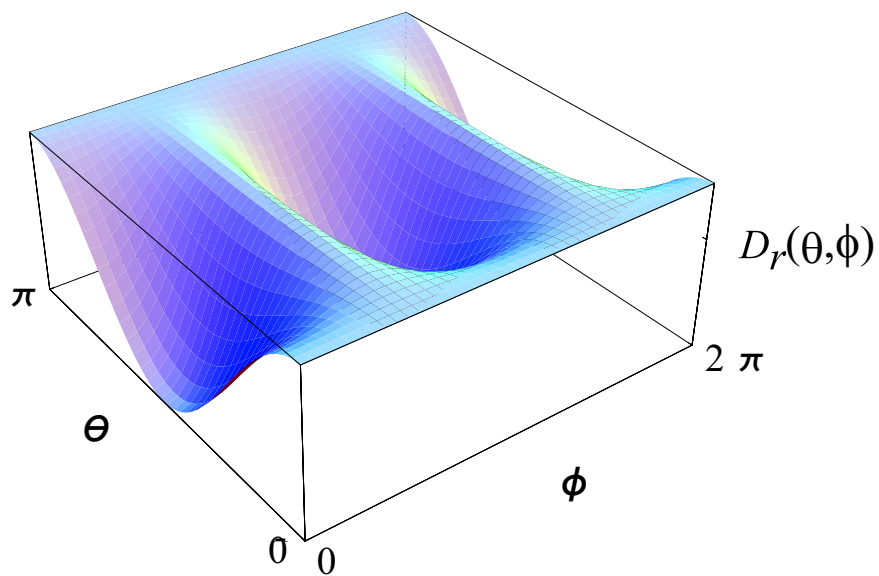


Figure 4.2: First-order directionally dependant diffusion, $D_r(\theta, \phi)$, for uniaxial fiber alignment along the x_1 axis (normalized with $\|\dot{\gamma}\| = 1$).

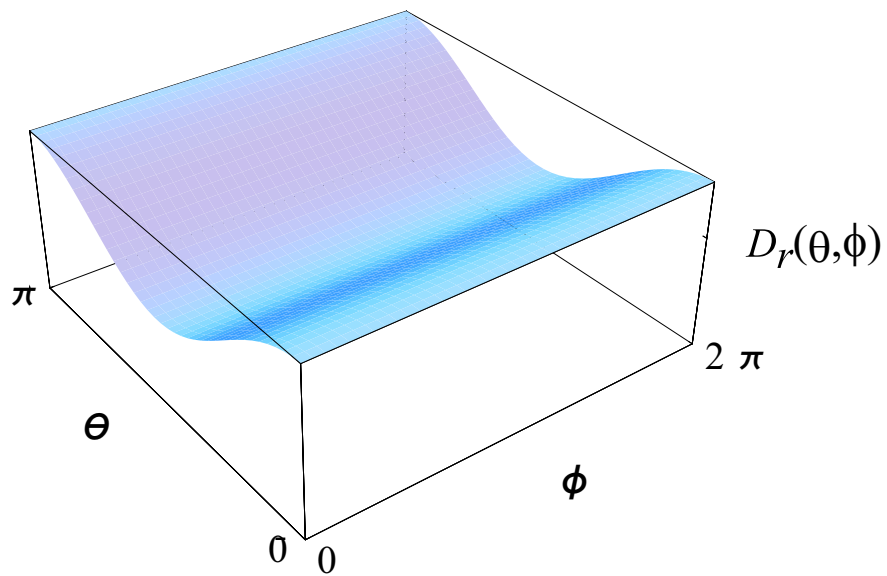


Figure 4.3: Directionally dependant diffusion for randomly orientated fiber distribution in the $x_1 - x_2$ plane (normalized with $\|\dot{\gamma}\| = 1$).

Simplifying the above by recognizing D_1 and D_2 are constant parameters,

$$\begin{aligned}
\frac{DA_{\alpha\beta}}{Dt} &= -\frac{1}{2}\omega_{\alpha j}A_{j\beta} + \frac{1}{2}A_{\alpha j}\omega_{j\beta} + \frac{1}{2}\lambda(\dot{\gamma}_{\alpha j}A_{j\beta} + A_{\alpha j}\dot{\gamma}_{j\beta} - 2\dot{\gamma}_{ij}A_{ij\alpha\beta}) \\
&\quad + \|\dot{\gamma}\| D_1 \left(2\delta_{\alpha\beta} \oint_{\mathbb{S}^2} \psi d\mathbb{S} - 6 \oint_{\mathbb{S}^2} \psi r_\alpha r_\beta d\mathbb{S} \right) \\
&\quad + \|\dot{\gamma}\| D_2 \left(2 \oint_{\mathbb{S}^2} r_k r_l \delta_{\alpha\beta} \psi d\mathbb{S} - 6 \oint_{\mathbb{S}^2} r_k r_l r_\alpha r_\beta \psi d\mathbb{S} \right)
\end{aligned} \tag{4.3}$$

which is trivially simplified using the definition of the orientation tensors from Equation (2.8) as

$$\begin{aligned}
\frac{DA_{\alpha\beta}}{Dt} &= -\frac{1}{2}\omega_{\alpha j}A_{j\beta} + \frac{1}{2}A_{\alpha j}\omega_{j\beta} + \frac{1}{2}\lambda(\dot{\gamma}_{\alpha j}A_{j\beta} + A_{\alpha j}\dot{\gamma}_{j\beta} - 2\dot{\gamma}_{ij}A_{ij\alpha\beta}) \\
&\quad + 2\|\dot{\gamma}\| D_1 (\delta_{\alpha\beta} - 3A_{\alpha\beta}) + 2\|\dot{\gamma}\| D_2 (A_{kl}\delta_{\alpha\beta} - 3A_{kl\alpha\beta})
\end{aligned} \tag{4.4}$$

Observe how knowledge of the fourth-order orientation tensor A_{ijkl} is necessary to solve the evolution equation of the second-order orientation tensor A_{ij} . Therefore for any orientation tensor flow simulations, it is necessary to select a fourth-order closure to approximate A_{ijkl} as a function of A_{ij} . Unfortunately, most of the largely accepted fourth-order closures are fit to data from the fiber orientation probability distribution function solution assuming the Folgar and Tucker model for diffusion [11, 12, 14, 16–19, 22, 52]. Conversely, the class of closures developed independent of fiber distribution function flow results is small [2, 7, 59, 66, 70]. The preliminary model for directionally dependant diffusion is presented using the established orthotropic closure employed by VerWeyst and Tucker [31] due to the way the closure is constructed. Most closures tend to experience numerical instability for predicted orientation states that fall outside the physical regime. The physical regime is defined by taking the eigenvalues of the second-order orientation tensor defined as $A_{(1)}$, $A_{(2)}$ and $A_{(3)}$ and

are taken such that $A_{(1)} \geq A_{(2)} \geq A_{(3)} \geq 0$. Recognizing that $A_{(1)} + A_{(2)} + A_{(3)} = 1$, there are only two independent eigenvalues of A_{ij} such that all possible orientation states are contained within the shaded region of Figure 4.4. The orthotropic closure used by VerWeyst [71] is constructed such that orientation states of A_{ij} occurring just outside the shaded region of Figure 4.4 will yield values for A_{ijkl} that can produce a physically conceivable orientation state for A_{ijkl} . This is done by fitting a function for $A_{ijkl} \approx f_{ijkl}(A_{mn})$, such that the slope of the function f_{ijkl} is significant just outside the shaded region in Figure 4.4.

Another orthotropic closure introduced by Wetzel [59] and the Rational Closure of Chaubal and Leal [70] may be valid closures for the first-order directional diffusion model since they are both formed based upon orientation states found in typical molding processes. The Wetzel closure is not investigated here due to the popularity of his second closure which is used in the following example. The Rational Closure is formed based upon the class of Bingham distributions [72] which have shown an exceptional capability to represent distribution functions seen in typical injection molding processes. Unfortunately, the Rational Closure has yet to be employed in short-fiber injection molding processes and will not be pursued further.

4.1.3 Orientation Tensor Evolution Results

Experimentally, orientation tensor components are obtained based upon measurements of the orientation of each fiber along a single cut of a sample, and results are volume averaged at each cut [6, 34, 73]. The Folgar and Tucker model is numerically

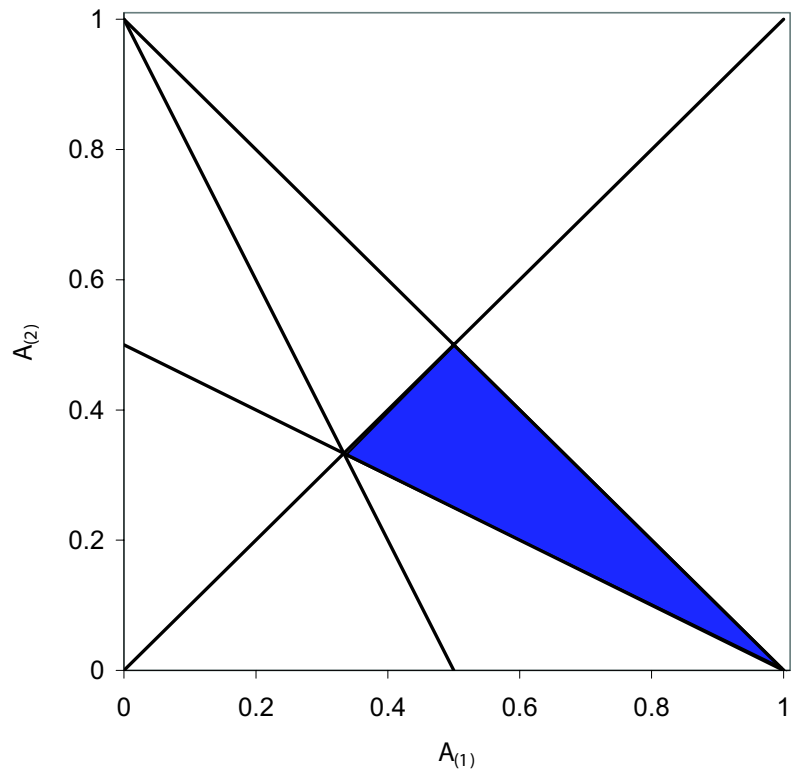


Figure 4.4: Eigenspace of possible orientations of the second-order orientation tensor.

solved with the parameter C_I being adjusted until the best fit for the steady state solution is obtained [1]. Results for the preliminary diffusion model are fit to the steady state results obtained from the Folgar and Tucker model for a given volume fraction and flow condition. To do this, a Fortran code has been developed by the author based on that of Bay [34] for solving the distribution function evolution of fibers using a control volume method, and results from the program have been validated through comparisons with those in the literature (see Jack [46]).

To solve the orientation tensor flow equation from Equation (4.4), a program has been written in Intel Visual Fortran 9.0 [74] within Microsoft Visual Studio.NET 2003 [75] that solves the second-order orientation tensor flow equations with the first-order directionally dependant diffusion model using the orthotropic closure of Wetzel [59] as discussed by VerWeyst and Tucker [31]. The five independent components of the second-order orientation tensor, A_{11} , A_{12} , A_{13} , A_{22} , and A_{23} , are solved using a fourth-order Runge-Kutta solution method (see e.g. [76]) for a given aspect ratio, fiber volume fraction, along with values for D_1 and D_2 and the steady state results for a particular flow field are computed. The steady state solution is adjusted from the preliminary diffusion model through the parameter D_1 the steady state results correspond with those presented in the Folgar and Tucker model.

4.1.3.1 Results for $D_2 = -10^{-1}$: Simple Shear Flow

To form an understanding of the behavior of the preliminary diffusion model, a representative case is selected with $\lambda = 1$ and $V_f = 15\%$. The surrounding fluid experiences simple shear flow schematically shown in Figure 4.5, where the only flow is in the x_1

direction with changes in the x_3 direction along the x_1 axis, i.e. $v_1 = Gx_3$ and $v_2 = v_3 = 0$ where G is a scaling parameter. Without any diffusion, Jeffery's model predicts non-interacting fibers tend to align along the x_1 axis at steady state. Due to interaction effects, fibers will tend toward alignment along the x_1 axis but the fiber distribution never experiences full alignment, but may attain high alignments dependant upon the volume fraction of fibers. For the case with $V_f = 15\%$, the expected second-order orientation tensor at steady state would be similar to,

$$A_{ij} = \begin{bmatrix} 0.773 & 0.0 & 0.083 \\ 0.0 & 0.152 & 0.0 \\ 0.083 & 0.0 & 0.075 \end{bmatrix} \quad (4.5)$$

As discussed previously, there are five independent components of A_{ij} . The only case where the steady state results for A_{ij} from the proposed model will be identical to those of the Folgar and Tucker model will be the trivial case when $D_1 = C_I$ and $D_2 = 0$, otherwise the final orientation state will differ to some degree. Therefore only one parameter will be selected to base the selection of D_1 and D_2 upon. The choice is the largest component of A_{ij} since the experimental error is the least for the largest component of the second-order orientation tensor [34]. For the case of simple shear, this is the A_{11} component. A simple search algorithm yielded that for $D_2 = -0.1$, a value of $D_1 = 8.85 \times 10^{-2}$ will produce the same steady state for A_{11} as that obtained with the Folgar and Tucker model. The results are seen in Figure 4.6 for two components of A_{ij} . Clearly, the steady state results are the same for the A_{11} components from the two methods, but the results for A_{22} differ between the two methods as do other components of A_{ij} . Notice, the first-order directional diffusion model tends to slow down the alignment process as seen by the rate at which steady

state is obtained for both the Folgar and Tucker model and the first-order directional diffusion model. The process was repeated for $D_2 = -0.2$, but numerical solutions rapidly diverged from the physical bounds shown in Figure 4.4. A value for D_1 could never be found to satisfy the criteria for the steady state value for A_{11} being similar to that predicted in the Folgar and Tucker model.

4.1.3.2 Results for $D_1 = D_1(D_2)$: Simple Shear Flow

The process discussed above for selecting a value of D_2 , then finding the correct D_1 to obtain the steady state results was repeated for a range of values for D_2 . A simple Fortran code was formulated that invokes the Newton-Raphson method of optimization with an adaptive step size. The adaptive step size helped to ensure results remained within the eigenspace for the second-order orientation tensor presented in Figure 4.4. The algorithm employed to perform the optimization is based upon that of Griffiths and Smith [77], and is written to automatically step through a range of values for D_2 in increments of -10^{-3} starting with zero to determine the best fit value of D_1 to render the correct steady state results. It was found that convergence to a solution for D_1 was difficult, if not impossible, for values of $D_2 \leq -1.6 \times 10^{-1}$ since the numerical solution would leave the physical regime for A_{ij} . The results for select points of D_2 between -1.6×10^{-1} and 0 are shown in Figure 4.7. Selected results for $D_1(D_2)$ are given as the circles in the figure with a linear curve fit between the points using a simple linear least squares fit (see e.g. [76]) found as

$$D_1 = -7.84 \times 10^{-1} D_2 + 10^{-2} \tag{4.6}$$

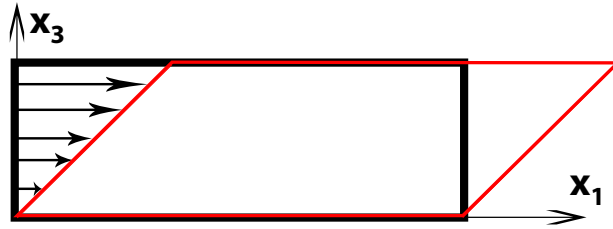


Figure 4.5: Schematic of simple shear flow with shearing in the x_3 direction along the x_1 axis.

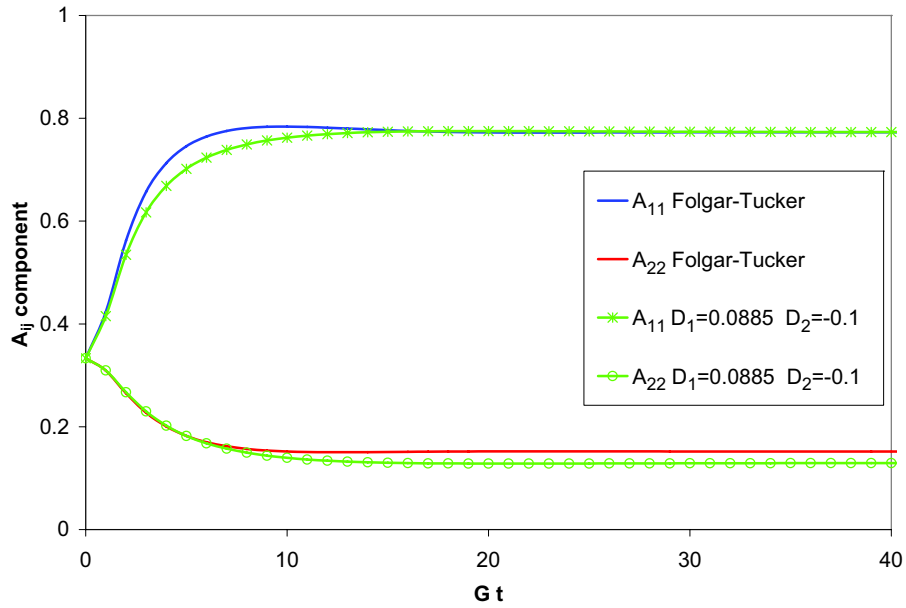


Figure 4.6: Results from simple-shear flow demonstrating steady state results for $D_1 = 8.85 \times 10^{-2}$ and $D_2 = 10^{-1}$.

with an R^2 value of 9.9992×10^{-1} where $R^2 = 1$ designates a perfect linear fit.

4.1.3.3 Results for $D_1 = D_1(D_2)$: Uniaxial Elongation Flow

The preliminary model yields the desired behavior for delaying the fiber alignment, but results do not yield a conclusive choice for which flow to base the model upon. For example, consider the case of uniaxial elongational flow where $v_1 = Gx_1$, $v_2 = -\frac{1}{2}Gx_2$, and $v_3 = -\frac{1}{2}Gx_3$. As in the preceding case for simple shear flow, the fiber distribution will tend to orient along the x_1 axis, but due to the fiber interactions will not reach perfect alignment. The fiber distribution for uniaxial elongation flow will tend to have a greater degree of fiber alignment than the preceding example for simple shear flow, therefore the A_{11} component will be greater for uniaxial elongation. A set of values for D_2 were chosen ranging from $-1.6 \times 10^{-1} \leq D_2 \leq 0$ and the values of D_1 were determined using the aforementioned Fortran program. Select results are given in Figure 4.8 along with a linear least squares fit. The data presents a near perfect linear fit between D_1 and D_2 as

$$D_1 = -9.45 \times 10^{-1}D_2 + 10^{-2} \quad (4.7)$$

with an R^2 value of 9.9998×10^{-1} .

4.1.4 Impediment for Preliminary Diffusion Model

The first-order directional diffusion model coefficients D_1 and D_2 provide a set of scalable parameters and provide a means to attain similar steady state results as the Folgar and Tucker model, while slowing down the rate of alignment. The difficulty is the uncertainty in the accuracy of the model. Since the Folgar and Tucker diffusion

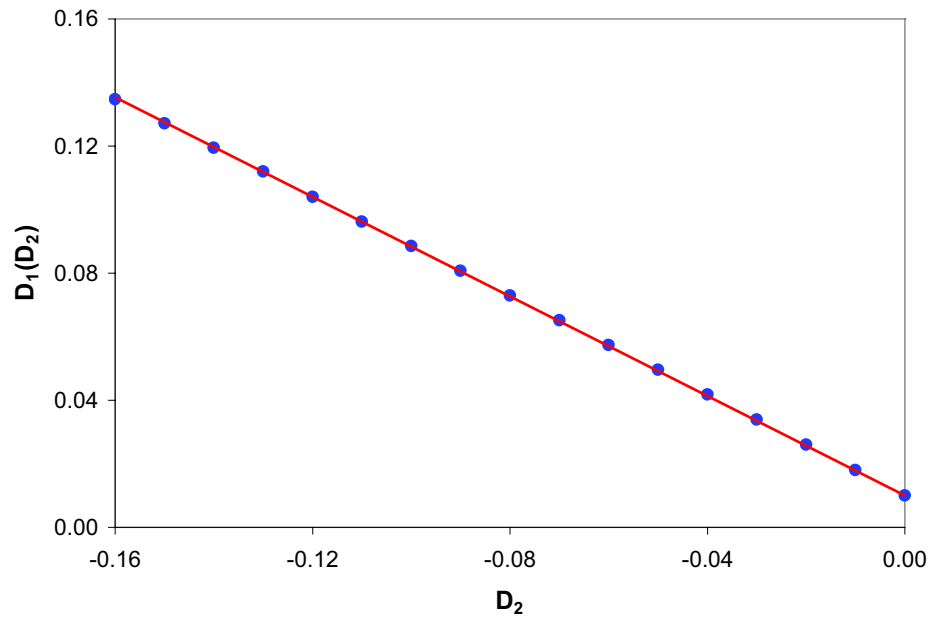


Figure 4.7: Results demonstrating the excellent correlation between optimal relation for D_1 given D_2 and linear least squares fit from simple shear flow.

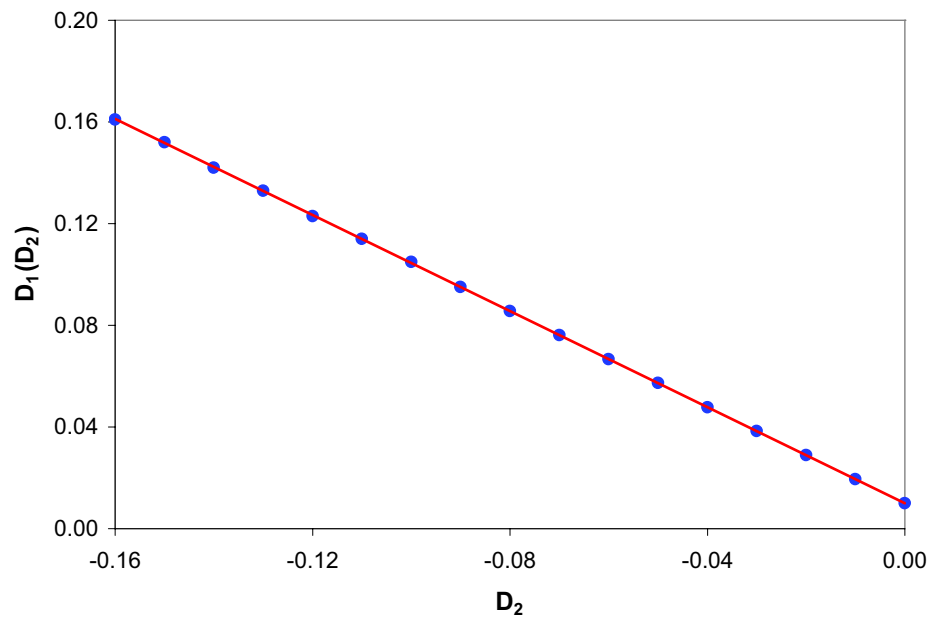


Figure 4.8: Results demonstrating the excellent correlation between optimal relation for D_1 given D_2 and linear least squares fit from uniaxial elongation flow.

model is fit to the steady state orientation results for the full fiber distribution, not just a single component of the second-order orientation tensor, it is believed that singling out a single component may lead to unsatisfactory results. Additional concerns lie in the clear discrepancy between the functional relationship between D_1 and D_2 based upon the two investigated flows. It is desirable to present a model that does not rely upon the choice of flow field, and is general enough to satisfy a wide range of typically encountered flow behavior. Unfortunately, the preliminary model is unable to satisfy this stipulation. An additional concern lies with the inability of the present model to sufficiently diminish the rate of alignment. As the parameter D_2 is increased, thus diminishing the alignment rate, the orientation results demonstrated a stronger propensity to display numerical instabilities. It was observed that when D_2 was selected less than -1.0 in simple shear flow, and an initial orientation state with alignment state greater than the desired steady state results from Equation (4.5) (i.e. $A_{11} = 0.8$, $A_{22} = A_{33} = 0.1$, and $A_{ij} = 0 \forall i \neq j$) the solution would rapidly produce nonphysical results. Therefore, with the low capability to diminish the alignment rate and the orientational difficulties in high alignment states, further investigation of the first-order directionally dependant diffusion model presented in Equation (4.1) is discarded in favor of the advanced model for directional diffusion discussed in the following section.

4.2 Advanced Model for Directional Diffusion

The preliminary first-order model for directional diffusion is not sufficient for actual industrial applications. It provides little more than a means to introduce minor levels of directionally biased diffusion. The advanced model for directional diffusion is based upon the incorporation of two effects, a local bias toward directional effects directly caused by the collision of two fibers, and large scale volume averaged diffusion behavior similar to Brownian motion.

4.2.1 Development of Advanced Directional Diffusion Model

The model for local effects between two fibers originates with two fibers defined by the unit vectors \mathbf{r} and $\boldsymbol{\rho}$, as shown in Figure 4.9. During a small period of time Δt the fiber $\boldsymbol{\rho}$ rotates by an angle proportionate to $\dot{\boldsymbol{\rho}}^h$, where $\dot{\boldsymbol{\rho}}^h$ is the time rate of change of the fiber $\boldsymbol{\rho}$ given by Jeffery's model from Equation (2.14). For very small periods of time, the area through which $\boldsymbol{\rho}$ rotates is proportionate to the length of $\boldsymbol{\rho} \times \dot{\boldsymbol{\rho}}^h$ within some constant proportionate to the fiber length and the period of time Δt . Notice that the resultant vector corresponds with the vector normal to the plane cut out by the fiber during the time Δt . Recognizing this, and observing that the probability of a hit between \mathbf{r} and $\boldsymbol{\rho}$ will be zero when \mathbf{r} is parallel with the plane made by $\boldsymbol{\rho}$ during Δt and will be greatest when \mathbf{r} is perpendicular to the plane made by $\boldsymbol{\rho}$. It is apparent that the probability of collision must incorporate this observation through the dot product of \mathbf{r} with the normal vector of the plane made by $\boldsymbol{\rho}$ and $\dot{\boldsymbol{\rho}}^h$ as $\mathbf{r} \cdot (\boldsymbol{\rho} \times \dot{\boldsymbol{\rho}}^h)$. Taking the absolute value of this quantity yields the scalar triple product [78] which

provides the volume of the parallelepiped determined by the vectors \mathbf{r} , $\boldsymbol{\rho}$ and $\dot{\boldsymbol{\rho}}^h$. It is proposed that the probability of $\boldsymbol{\rho}$ hitting \mathbf{r} , $P_{\boldsymbol{\rho} \text{ hit } \mathbf{r}}$, during the small time Δt is proportional to the volume of the parallelepiped. By pre-multiplying by the constant C_1 , which can be a function of the fiber aspect ratio r_e and the volume fraction of fibers V_f , the probability of a collision during Δt is given by

$$P_{\boldsymbol{\rho} \text{ hit } \mathbf{r}} = C_1 |\mathbf{r} \cdot (\boldsymbol{\rho} \times \dot{\boldsymbol{\rho}}^h)| \quad (4.8)$$

Note that the magnitude of the scalar triple product for the vectors $\mathbf{a}, \mathbf{b}, \mathbf{c} \in \mathbb{R}^3$ obey the relationship $|\mathbf{a} \cdot (\mathbf{b} \times \mathbf{c})| = |\mathbf{b} \cdot (\mathbf{c} \times \mathbf{a})| = |\mathbf{c} \cdot (\mathbf{a} \times \mathbf{b})| = |\mathbf{a} \cdot (\mathbf{c} \times \mathbf{b})| = \dots$ [79], the probability of $\boldsymbol{\rho}$ hitting \mathbf{r} is rewritten as

$$P_{\boldsymbol{\rho} \text{ hit } \mathbf{r}} = C_1 |\boldsymbol{\rho} \cdot (\mathbf{r} \times \dot{\boldsymbol{\rho}}^h)| \quad (4.9)$$

During the same time, Δt , the fiber \mathbf{r} will experience motion of its own, $\dot{\mathbf{r}}^h$, given by Jeffery's model from Equation (2.14). In a similar manner, it is observed that the probability of the fiber \mathbf{r} hitting $\boldsymbol{\rho}$ is provided by the relationship

$$P_{\mathbf{r} \text{ hit } \boldsymbol{\rho}} = C_1 |\mathbf{r} \cdot (\boldsymbol{\rho} \times \dot{\mathbf{r}}^h)| \quad (4.10)$$

where C_1 is the same constant given in Equation (4.9) since the probability of \mathbf{r} hitting $\boldsymbol{\rho}$ is the same as the probability of $\boldsymbol{\rho}$ hitting \mathbf{r} . This procedure is summed for each fiber within the sphere surrounding the fiber \mathbf{r} . Since each of the fibers $\boldsymbol{\rho}$ are taken from the fiber orientation probability distribution function $\psi(\boldsymbol{\rho})$, the expectation of the collisions may be replaced by the integral over $\boldsymbol{\rho} \in \mathbb{S}^2$ to represent the directional

diffusion due to local fiber collision effects as

$$D_r(\theta, \phi) \Big|_{\text{Local Collisions}} = \oint_{\boldsymbol{\rho} \in \mathbb{S}^2} (C_1 |\boldsymbol{\rho} \cdot (\mathbf{r} \times \dot{\boldsymbol{\rho}}^h)| + C_1 |\mathbf{r} \cdot (\boldsymbol{\rho} \times \dot{\mathbf{r}}^h)|) \psi(\boldsymbol{\rho}) \, d\mathbb{S} \quad (4.11)$$

The volume averaged effects are assumed to satisfy the Brownian type behavior observed by Folgar and Tucker [1], and will be modeled as

$$D_r(\theta, \phi) \Big|_{\text{Brownian}} = \oint_{\boldsymbol{\rho} \in \mathbb{S}^2} C_2 \|\dot{\boldsymbol{\gamma}}\| \psi(\boldsymbol{\rho}) \, d\mathbb{S} \quad (4.12)$$

Incorporating these effects produce the desired results presented in the introduction, even though their formulation is not fully understood and will be a topic of future research.

The proposed model incorporates the diffusion due to local collisions and Brownian motion to express the rotary diffusion D_r from Equation (2.18) as a sum of the two effects as

$$D_r(\theta, \phi) = \oint_{\boldsymbol{\rho} \in \mathbb{S}^2} (C_1 |\boldsymbol{\rho} \cdot (\mathbf{r} \times \dot{\boldsymbol{\rho}}^h)| + C_1 |\mathbf{r} \cdot (\boldsymbol{\rho} \times \dot{\mathbf{r}}^h)|) \psi(\boldsymbol{\rho}) \, d\mathbb{S} + \oint_{\boldsymbol{\rho} \in \mathbb{S}^2} C_2 \|\dot{\boldsymbol{\gamma}}\| \psi(\boldsymbol{\rho}) \, d\mathbb{S} \quad (4.13)$$

Observe the rotary diffusion D_r in Equation (4.13) integrates over the unit sphere associated with the fiber $\boldsymbol{\rho}$ and accounts for interactions with each of the fibers surrounding $\boldsymbol{\rho}$. Each of the terms \mathbf{r} , $\boldsymbol{\rho}$, $\dot{\mathbf{r}}^h$, and $\dot{\boldsymbol{\rho}}^h$ have already been assumed continuous and finite as is the rate of deformation tensor $\|\dot{\boldsymbol{\gamma}}\|$, therefore the integration in Equation (4.13) exists and is finite, and can be expressed as

$$\begin{aligned} D_r(\theta, \phi) &= C_1 \oint_{\boldsymbol{\rho} \in \mathbb{S}^2} |\boldsymbol{\rho} \cdot (\mathbf{r} \times \dot{\boldsymbol{\rho}}^h)| \psi(\boldsymbol{\rho}) \, d\mathbb{S} + C_1 \oint_{\boldsymbol{\rho} \in \mathbb{S}^2} |\mathbf{r} \cdot (\boldsymbol{\rho} \times \dot{\mathbf{r}}^h)| \psi(\boldsymbol{\rho}) \, d\mathbb{S} \\ &\quad + C_2 \oint_{\boldsymbol{\rho} \in \mathbb{S}^2} \|\dot{\boldsymbol{\gamma}}\| \psi(\boldsymbol{\rho}) \, d\mathbb{S} \end{aligned} \quad (4.14)$$

The absolute values within the integration pose a significant problem in finding an analytical form for the diffusion expressed in terms of the orientation tensors (recall $A_{ij\dots} = \oint_{\mathbb{S}^2} r_i r_j \dots d\mathbb{S}$). Therefore it is desired to approximate the function $f(x) = |x|$ by the function $g(x) = x^2$ for $x \in [-1, 1]$. Observe from Figure 4.10 that this approximation tends to under predict the actual value of the function $f(x)$ except for $x = -1, 0, 1$. Therefore, when this approximation is used for the integrations in Equation (4.14) will tend underpredict the actual number of local collisions. This concern is noted and is accepted in comparison to neglecting the directional nature of diffusion entirely.

Implicit within the approximation to replace $|x|$ with x^2 is the value of the function $f(x)$ must remain between -1 and 1. Observing the scalar triple products from Equation (4.14), each component of the unit vectors \mathbf{r} and $\boldsymbol{\rho}$ will always be equal to or less than one in magnitude. The only terms to be concerned with are $\dot{\mathbf{r}}^h$ and $\dot{\boldsymbol{\rho}}^h$ since they experience no such bounds. Recall from Equation (2.14) that each component in $\dot{\mathbf{r}}^h$ (or $\dot{\boldsymbol{\rho}}^h$) is a product of components of \mathbf{r} (or $\boldsymbol{\rho}$) multiplied by either the rate of deformation tensor γ_{ij} or the vorticity tensor ω_{ij} . Since any product of the components of \mathbf{r} (or $\boldsymbol{\rho}$) will be less than one in magnitude, the only terms to be of concern are γ_{ij} and ω_{ij} . Each of these terms are always equal to or less than the scalar magnitude of the rate of deformation tensor $\|\dot{\boldsymbol{\gamma}}\| = \sqrt{\frac{1}{2} \dot{\gamma}_{ij} \dot{\gamma}_{ji}}$. Therefore each of terms within $\left| \boldsymbol{\rho} \cdot \left(\mathbf{r} \times \frac{\dot{\boldsymbol{\rho}}^h}{\|\dot{\boldsymbol{\gamma}}\|} \right) \right|$ and $\left| \mathbf{r} \cdot \left(\boldsymbol{\rho} \times \frac{\dot{\mathbf{r}}^h}{\|\dot{\boldsymbol{\gamma}}\|} \right) \right|$ are less than 1 for all values

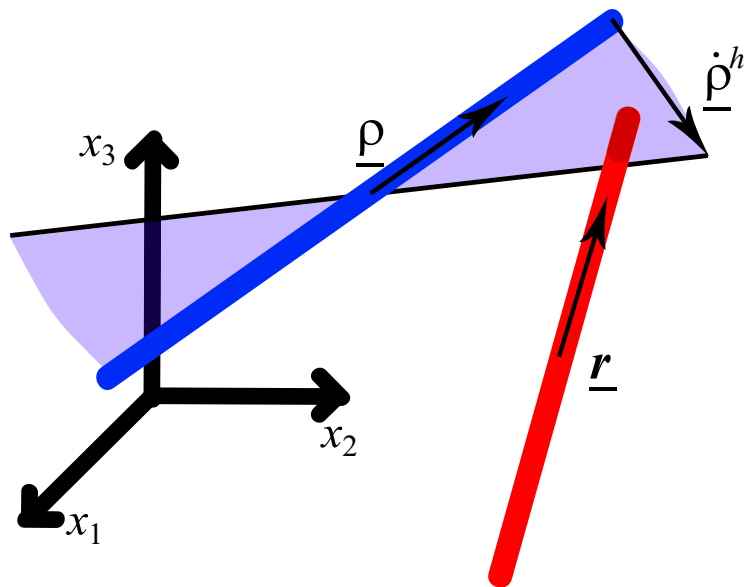


Figure 4.9: Coordinate system describing the path through which the fiber ρ passes into and r .

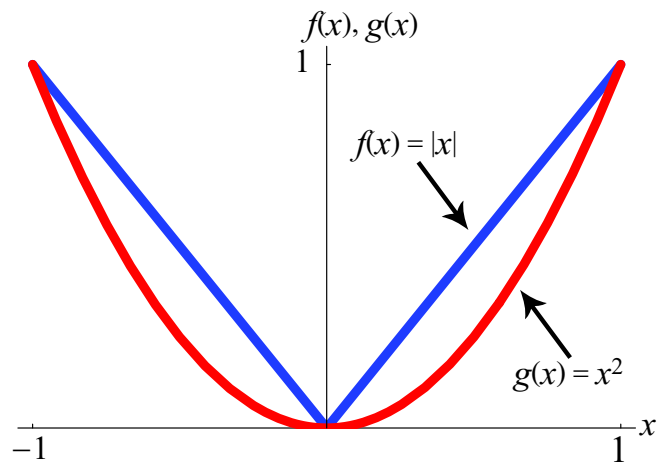


Figure 4.10: Comparison between $f(x) = |x|$ and $g(x) = x^2$ for $x \in [-1, 1]$.

of \mathbf{r} and $\boldsymbol{\rho}$ and for all velocity gradients. Equation (4.14) is then approximated as

$$\begin{aligned}
D_r(\theta, \phi) &= C_1 \|\dot{\boldsymbol{\gamma}}\| \oint_{\boldsymbol{\rho} \in \mathbb{S}^2} \left| \boldsymbol{\rho} \cdot \left(\mathbf{r} \times \frac{\dot{\boldsymbol{\rho}}^h}{\|\dot{\boldsymbol{\gamma}}\|} \right) \right| \psi(\boldsymbol{\rho}) \, d\mathbb{S} \\
&\quad + C_1 \|\dot{\boldsymbol{\gamma}}\| \oint_{\boldsymbol{\rho} \in \mathbb{S}^2} \left| \mathbf{r} \cdot \left(\boldsymbol{\rho} \times \frac{\dot{\mathbf{r}}^h}{\|\dot{\boldsymbol{\gamma}}\|} \right) \right| \psi(\boldsymbol{\rho}) \, d\mathbb{S} + C_2 \oint_{\boldsymbol{\rho} \in \mathbb{S}^2} \|\dot{\boldsymbol{\gamma}}\| \psi(\boldsymbol{\rho}) \, d\mathbb{S} \\
&\approx C_1 \|\dot{\boldsymbol{\gamma}}\| \oint_{\boldsymbol{\rho} \in \mathbb{S}^2} \left(\boldsymbol{\rho} \cdot \left(\mathbf{r} \times \frac{\dot{\boldsymbol{\rho}}^h}{\|\dot{\boldsymbol{\gamma}}\|} \right) \right)^2 \psi(\boldsymbol{\rho}) \, d\mathbb{S} \\
&\quad + C_1 \|\dot{\boldsymbol{\gamma}}\| \oint_{\boldsymbol{\rho} \in \mathbb{S}^2} \left(\mathbf{r} \cdot \left(\boldsymbol{\rho} \times \frac{\dot{\mathbf{r}}^h}{\|\dot{\boldsymbol{\gamma}}\|} \right) \right)^2 \psi(\boldsymbol{\rho}) \, d\mathbb{S} + C_2 \oint_{\boldsymbol{\rho} \in \mathbb{S}^2} \|\dot{\boldsymbol{\gamma}}\| \psi(\boldsymbol{\rho}) \, d\mathbb{S} \quad (4.15)
\end{aligned}$$

The scalar triple product can be expressed for the vectors \mathbf{a} , \mathbf{b} , and \mathbf{c} in index notation as $\mathbf{a} \cdot (\mathbf{b} \times \mathbf{c}) = \epsilon_{ijk} a_i b_j c_k$ where ϵ_{ijk} is the permutation symbol defined as [80]

$$\epsilon_{ijk} = \begin{cases} 0 & i = j, \text{ or } j = k, \text{ or } k = i \\ +1 & (i, j, k) \in \{(1, 2, 3), (2, 3, 1), (3, 1, 2)\} \\ -1 & (i, j, k) \in \{(1, 3, 2), (3, 2, 1), (2, 1, 3)\} \end{cases} \quad (4.16)$$

The last term of Equation (4.15) can be simply expressed as $C_2 \|\dot{\boldsymbol{\gamma}}\|$ recognizing that both C_2 and $\|\dot{\boldsymbol{\gamma}}\|$ are independent of the integration, and $\oint_{\boldsymbol{\rho} \in \mathbb{S}^2} \psi(\boldsymbol{\rho}) \, d\mathbb{S} = 1$.

Therefore, Equation (4.15) is written in index notation as

$$\begin{aligned}
D_r(\theta, \phi) &= \frac{C_1 \|\dot{\boldsymbol{\gamma}}\|}{\|\dot{\boldsymbol{\gamma}}\|^2} \oint_{\boldsymbol{\rho} \in \mathbb{S}^2} (\epsilon_{ijk} \rho_i r_j \dot{\rho}_k^h)^2 \psi(\boldsymbol{\rho}) \, d\mathbb{S} \\
&\quad + \frac{C_1 \|\dot{\boldsymbol{\gamma}}\|}{\|\dot{\boldsymbol{\gamma}}\|^2} \oint_{\boldsymbol{\rho} \in \mathbb{S}^2} (\epsilon_{ijk} r_i \rho_j \dot{r}_k^h)^2 \psi(\boldsymbol{\rho}) \, d\mathbb{S} + C_2 \|\dot{\boldsymbol{\gamma}}\| \quad (4.17)
\end{aligned}$$

For the remainder of this section, the usual index summation is suspended for the indices i , j and k . Then using Jeffery's model from Equation (2.14), to represent the

motion of \mathbf{r} and $\boldsymbol{\rho}$, the squares can be expanded as

$$\begin{aligned}
D_r(\theta, \phi) &= \frac{C_1}{\|\dot{\boldsymbol{\gamma}}\|} (\epsilon_{ijk})^2 r_j r_j \oint_{\boldsymbol{\rho} \in \mathbb{S}^2} (\rho_i \rho_i \dot{\rho}_k^h \dot{\rho}_k^h) \psi(\boldsymbol{\rho}) \, d\mathbb{S} \\
&\quad + \frac{C_1}{\|\dot{\boldsymbol{\gamma}}\|} (\epsilon_{ijk})^2 r_i r_i \dot{r}_k^h \dot{r}_k^h \oint_{\boldsymbol{\rho} \in \mathbb{S}^2} \rho_j \rho_j \psi(\boldsymbol{\rho}) \, d\mathbb{S} + C_2 \|\dot{\boldsymbol{\gamma}}\| \\
&= \frac{C_1}{\|\dot{\boldsymbol{\gamma}}\|} (\epsilon_{ijk})^2 r_j r_j \oint_{\boldsymbol{\rho} \in \mathbb{S}^2} \left(\rho_i \rho_i \left(-\frac{1}{2} \omega_{kl} \rho_l + \frac{1}{2} \lambda (\dot{\gamma}_{kl} \rho_l - \dot{\gamma}_{lm} \rho_l \rho_m \rho_k) \right) \right. \\
&\quad \left. \left(-\frac{1}{2} \omega_{kn} \rho_n + \frac{1}{2} \lambda (\dot{\gamma}_{kn} \rho_n - \dot{\gamma}_{no} \rho_n \rho_o \rho_k) \right) \right) \psi(\boldsymbol{\rho}) \, d\mathbb{S} \\
&\quad + \frac{C_1}{\|\dot{\boldsymbol{\gamma}}\|} (\epsilon_{ijk})^2 r_i r_i \dot{r}_k^h \dot{r}_k^h A_{jj} + C_2 \|\dot{\boldsymbol{\gamma}}\| \tag{4.18}
\end{aligned}$$

where the definition of the orientation tensors from Equation (2.8) was used to simplify

$\oint_{\boldsymbol{\rho} \in \mathbb{S}^2} \rho_j \rho_j \psi(\boldsymbol{\rho}) \, d\mathbb{S} = A_{jj}$. Equation (4.18) can be further expressed as

$$\begin{aligned}
D_r(\theta, \phi) &= \frac{C_1}{\|\dot{\boldsymbol{\gamma}}\|} (\epsilon_{ijk})^2 r_j r_j \oint_{\boldsymbol{\rho} \in \mathbb{S}^2} \psi(\boldsymbol{\rho}) \rho_i \rho_i \left(\frac{1}{4} \omega_{kl} \omega_{kn} \rho_l \rho_n - \frac{1}{4} \lambda \omega_{kl} \dot{\gamma}_{ko} \rho_l \rho_o \right. \\
&\quad \left. + \frac{1}{4} \lambda \omega_{kl} \dot{\gamma}_{no} \rho_l \rho_n \rho_o \rho_k - \frac{1}{4} \lambda \omega_{kn} \dot{\gamma}_{kl} \rho_l \rho_n + \frac{1}{4} \lambda \omega_{kn} \dot{\gamma}_{lm} \rho_l \rho_m \rho_n \rho_k \right. \\
&\quad \left. + \frac{1}{4} \lambda^2 (\dot{\gamma}_{kl} \dot{\gamma}_{ko} \rho_l \rho_o - \dot{\gamma}_{kl} \dot{\gamma}_{no} \rho_l \rho_n \rho_o \rho_k - \dot{\gamma}_{ko} \dot{\gamma}_{lm} \rho_l \rho_m \rho_o \rho_k) \right. \\
&\quad \left. + \frac{1}{4} \lambda^2 \dot{\gamma}_{lm} \dot{\gamma}_{no} \rho_l \rho_m \rho_k \rho_n \rho_o \rho_k \right) \, d\mathbb{S} + \frac{C_1}{\|\dot{\boldsymbol{\gamma}}\|} (\epsilon_{ijk})^2 r_i r_i \dot{r}_k^h \dot{r}_k^h A_{jj} + C_2 \|\dot{\boldsymbol{\gamma}}\| \tag{4.19}
\end{aligned}$$

Recognizing that the indices l , m , n , and o are dummy indices, terms such as

$\frac{1}{4} \lambda \omega_{kl} \dot{\gamma}_{ko} \rho_l \rho_o$ and $\frac{1}{4} \lambda \omega_{kn} \dot{\gamma}_{kl} \rho_l \rho_n$ are identical thus simplifying Equation (4.19) as

$$\begin{aligned}
D_r(\theta, \phi) &= \frac{C_1}{\|\dot{\boldsymbol{\gamma}}\|} (\epsilon_{ijk})^2 r_j r_j \oint_{\boldsymbol{\rho} \in \mathbb{S}^2} \psi(\boldsymbol{\rho}) \rho_i \rho_i \left(\left(\frac{1}{4} \omega_{kl} \omega_{km} - \frac{1}{2} \lambda \omega_{kl} \dot{\gamma}_{km} + \frac{1}{4} \lambda^2 \dot{\gamma}_{kl} \dot{\gamma}_{km} \right) \rho_l \rho_m \right. \\
&\quad \left. + \left(\frac{1}{2} \omega_{kl} \dot{\gamma}_{mn} - \frac{1}{2} \lambda^2 \dot{\gamma}_{kl} \dot{\gamma}_{mn} \right) \rho_k \rho_l \rho_m \rho_n + \frac{1}{4} \lambda^2 \dot{\gamma}_{lm} \dot{\gamma}_{no} \rho_k \rho_k \rho_l \rho_m \rho_n \rho_o \right) \, d\mathbb{S} \\
&\quad + \frac{C_1}{\|\dot{\boldsymbol{\gamma}}\|} (\epsilon_{ijk})^2 r_i r_i \dot{r}_k^h \dot{r}_k^h A_{jj} + C_2 \|\dot{\boldsymbol{\gamma}}\| \tag{4.20}
\end{aligned}$$

which is simplified with the definition of the orientation tensors from Equation (2.8)

$$\begin{aligned}
D_r(\theta, \phi) = & \frac{C_1}{\|\dot{\boldsymbol{\gamma}}\|} (\epsilon_{ijk})^2 r_j r_j \left(\left(\frac{1}{4} \omega_{kl} \omega_{km} - \frac{1}{2} \lambda \omega_{kl} \dot{\gamma}_{km} + \frac{1}{4} \lambda^2 \dot{\gamma}_{kl} \dot{\gamma}_{km} \right) A_{iilm} \right. \\
& + \left. \left(\frac{1}{2} \omega_{kl} \dot{\gamma}_{mn} - \frac{1}{2} \lambda^2 \dot{\gamma}_{kl} \dot{\gamma}_{mn} \right) A_{iiklmn} + \frac{1}{4} \lambda^2 \dot{\gamma}_{lm} \dot{\gamma}_{no} A_{iikklmno} \right) \\
& + \frac{C_1}{\|\dot{\boldsymbol{\gamma}}\|} (\epsilon_{ijk})^2 r_i r_i \dot{r}_k^h \dot{r}_k^h A_{jj} + C_2 \|\dot{\boldsymbol{\gamma}}\|
\end{aligned} \tag{4.21}$$

Observe in Equation (4.21) how the diffusion is clearly a function of both the velocity gradients through the rate of deformation and vorticity tensors, and the fiber orientation through the unit vector \mathbf{r} . A concern with the diffusion model may arise with the expression $1/\|\dot{\boldsymbol{\gamma}}\|$ as the velocity gradients of the surrounding fluid go to zero. This concern is quickly taken care of through the products of the expressions for ω_{ij} and $\dot{\gamma}_{ij}$ which go to zero as quickly or quicker than does the scalar magnitude of the rate of deformation.

It is worthwhile to note that the Folgar and Tucker model for diffusion is readily obtained by setting $C_1 = 0$ and $C_2 = C_I$. Also note that the eighth-order orientation tensor $A_{ijklmnop}$ appears in the proposed diffusion model. As previously discussed, there currently exist no reasonable closure methods for predicting the eight-order orientation tensor. As will be introduced in the following section, the tenth-order orientation tensor will appear in the second-order orientation tensor evolution equation, thus introducing the possible need for new advanced closures.

4.2.2 Orientation Tensor Evolution Formulation

The model for fiber orientation flow with the advanced model for diffusion from Equation (4.21) will utilize the second-order orientation tensor flow equation of Equation

(3.2). The diffusion component of this equation, $\oint_{\mathbb{S}^2} D_r \psi (2\delta_{\alpha\beta} - 6r_\alpha r_\beta) d\mathbb{S}$, is expressed with the advanced directional diffusion model as

$$\begin{aligned}
& \oint_{\mathbf{r} \in \mathbb{S}^2} D_r \psi(\mathbf{r}) (2\delta_{\alpha\beta} - 6r_\alpha r_\beta) d\mathbb{S} = \\
& \frac{C_1}{\|\dot{\gamma}\|} (\epsilon_{ijk})^2 \oint_{\mathbf{r} \in \mathbb{S}^2} \psi(\mathbf{r}) (2\delta_{\alpha\beta} - 6r_\alpha r_\beta) r_j r_j \left(\left(\frac{1}{4} \omega_{kl} \omega_{km} - \frac{1}{2} \lambda \omega_{kl} \dot{\gamma}_{km} + \frac{1}{4} \lambda^2 \dot{\gamma}_{kl} \dot{\gamma}_{km} \right) A_{iilm} \right. \\
& \quad \left. + \left(\frac{1}{2} \omega_{kl} \dot{\gamma}_{mn} - \frac{1}{2} \lambda^2 \dot{\gamma}_{kl} \dot{\gamma}_{mn} \right) A_{iiklmn} + \frac{1}{4} \lambda^2 \dot{\gamma}_{lm} \dot{\gamma}_{no} A_{iikklnmo} \right) d\mathbb{S} \\
& + \frac{C_1}{\|\dot{\gamma}\|} (\epsilon_{ijk})^2 \oint_{\mathbf{r} \in \mathbb{S}^2} \psi(\mathbf{r}) (2\delta_{\alpha\beta} - 6r_\alpha r_\beta) r_i r_i \dot{r}_k^h \dot{r}_k^h A_{jj} d\mathbb{S} \\
& + \oint_{\mathbf{r} \in \mathbb{S}^2} \psi(\mathbf{r}) (2\delta_{\alpha\beta} - 6r_\alpha r_\beta) C_2 \|\dot{\gamma}\| d\mathbb{S} \tag{4.22}
\end{aligned}$$

The first and third integrands are trivial since \mathbf{r} and $\psi(\mathbf{r})$ are the only terms that are dependant upon the integration. The second integral is simplified in a similar fashion as in the preceding section with the terms \dot{r}_k^h being replaced with Jeffery's model from Equation (2.14) as

$$\begin{aligned}
& \oint_{\mathbf{r} \in \mathbb{S}^2} D_r \psi(\mathbf{r}) (2\delta_{\alpha\beta} - 6r_\alpha r_\beta) d\mathbb{S} = \\
& \frac{C_1}{\|\dot{\gamma}\|} (\epsilon_{ijk})^2 (2\delta_{\alpha\beta} A_{jj} - 6A_{jj\alpha\beta}) \left(\left(\frac{1}{4} \omega_{kl} \omega_{km} - \frac{1}{2} \lambda \omega_{kl} \dot{\gamma}_{km} + \frac{1}{4} \lambda^2 \dot{\gamma}_{kl} \dot{\gamma}_{km} \right) A_{iilm} \right. \\
& \quad \left. + \left(\frac{1}{2} \omega_{kl} \dot{\gamma}_{mn} - \frac{1}{2} \lambda^2 \dot{\gamma}_{kl} \dot{\gamma}_{mn} \right) A_{iiklmn} + \frac{1}{4} \lambda^2 \dot{\gamma}_{lm} \dot{\gamma}_{no} A_{iikklnmo} \right) \\
& + \frac{C_1}{\|\dot{\gamma}\|} (\epsilon_{ijk})^2 \oint_{\mathbf{r} \in \mathbb{S}^2} \psi(\mathbf{r}) (2\delta_{\alpha\beta} - 6r_\alpha r_\beta) r_i r_i \left(-\frac{1}{2} \omega_{kl} r_l + \frac{1}{2} \lambda (\dot{\gamma}_{kl} r_l - \dot{\gamma}_{lm} r_l r_m r_k) \right) \\
& \quad \left(-\frac{1}{2} \omega_{kn} r_n + \frac{1}{2} \lambda (\dot{\gamma}_{kn} r_n - \dot{\gamma}_{no} r_n r_o r_k) \right) A_{jj} d\mathbb{S} \\
& + C_2 \|\dot{\gamma}\| (2\delta_{\alpha\beta} - 6A_{\alpha\beta}) \tag{4.23}
\end{aligned}$$

where the definition of the orientation tensors from Equation (2.8) replaces the terms $\oint_{\mathbf{r} \in \mathbb{S}^2} r_i r_j \cdots d\mathbb{S}$ with $A_{ij\dots}$. After much simplification, Equation (4.23) may be expressed as

$$\begin{aligned}
\oint_{\mathbf{r} \in \mathbb{S}^2} D_r \psi(\mathbf{r}) (2\delta_{\alpha\beta} - 6r_\alpha r_\beta) d\mathbb{S} &= \frac{C_1}{\|\dot{\gamma}\|} (\epsilon_{ijk})^2 \\
&\left(\left(\frac{1}{4} \omega_{kl} \omega_{km} - \frac{1}{2} \lambda \omega_{kl} \dot{\gamma}_{km} + \frac{1}{4} \lambda^2 \dot{\gamma}_{kl} \dot{\gamma}_{km} \right) (4\delta_{\alpha\beta} A_{jj} A_{iilm} - 6A_{jj\alpha\beta} A_{iilm} - 6A_{jj} A_{\alpha\beta iilm}) \right. \\
&+ \left(\frac{1}{2} \lambda \omega_{kl} \dot{\gamma}_{mn} - \frac{1}{2} \lambda^2 \dot{\gamma}_{kl} \dot{\gamma}_{mn} \right) (4\delta_{\alpha\beta} A_{jj} A_{iiklmn} - 6A_{jj\alpha\beta} A_{iiklmn} - 6A_{jj} A_{\alpha\beta iiklmn}) \\
&+ \left. \frac{1}{4} \lambda^2 \dot{\gamma}_{lm} \dot{\gamma}_{no} (4\delta_{\alpha\beta} A_{jj} A_{iikklnmo} - 6A_{jj\alpha\beta} A_{iikklnmo} - 6A_{jj} A_{\alpha\beta iikklnmo}) \right) \\
&+ C_2 \|\dot{\gamma}\| (2\delta_{\alpha\beta} - 6A_{\alpha\beta})
\end{aligned} \tag{4.24}$$

This equation contains the Folgar and Tucker model when the coefficients C_1 and C_2 are set to 0 and C_I respectively. More importantly, the diffusion expression from Equation (4.24) produces a directional dependance upon the diffusion component of the fiber orientation evolution equations. Notice that each of the even-ordered orientation tensors up to the tenth order appear in the expression for diffusion, and as such may present complications to perform solutions of the second-order orientation tensor evolution equation.

4.2.3 Orientation Tensor Evolution Closure Selection

As in the example for the preliminary directionally dependant diffusion model, the selection of a closure for the higher order information is necessary to allow a solution of the fiber orientation analysis. It might appear that the fitted closures such as those belonging to orthotropic class might be useful [11, 15–18, 59], but they are fit to data for the orientation distribution function generated with the Folgar and Tucker model.

Instead an analytic closure is desired to bypass the procedure required to complete the fitting. The fourth-order hybrid closure of Advani and Tucker [2] still regularly enjoys use in industrial simulations [81,82], even though it has been demonstrated to yield results for fiber orientation with an accuracy slightly less than that of the orthotropic closures [46,83] when the Folgar and Tucker model for diffusion is employed. Recognizing this, the hybrid closure is chosen because of the increased accuracy over any closure developed independent of the form of the fiber orientation distribution function flow equation. The sixth-order hybrid closure introduced by Advani and Tucker [2] is selected to compute the sixth-order orientation tensor once the fourth- and second-order orientation tensors are known. There exists little mention in the literature of higher order closure methods. As such, an eight-order closure similar in form to the sixth-order quadratic closure of Doi [66] is introduced as

$$a_{ijklmnop} \approx a_{ijklmn}a_{op} \tag{4.25}$$

and a tenth-order closure to approximate the tenth-order orientation tensor as a function of the eighth-order orientation tensor is proposed as

$$a_{ijklmnopqr} \approx a_{ijklmnop}a_{qr} \tag{4.26}$$

where for Equations (4.25) and (4.26) only, $i, j, k, l, m, n, o, p, q, r \in \{1, 2, 3\}$. Note, both the eighth- and tenth-order closures do not satisfy the symmetry conditions from Equation (2.9), but neither do the commonly employed fourth- or sixth-order hybrid closures. An accurate closure method for the advanced diffusion model must account for the correct form of the orientation tensors. Conversely, each of the closures in

Equations (4.25) and (4.26) exactly solve the higher-order orientation tensors for unidirectional alignment states, but will tend to overpredict the alignment state for all other orientation states.

4.2.4 Orientation Tensor Evolution Results

As discussed previously, a full investigation of the proposed model must include experimental verification. In lieu of experimental results, the model will be verified based upon the steady state results obtained from the Folgar and Tucker model for various interaction coefficients, and it is left to future endeavors to investigate the applicability of the proposed model. Recall, the interaction coefficient C_I from the Folgar and Tucker model is selected to fit the experimentally measured steady state results [3, 6, 8, 10, 12, 16, 17, 34, 41, 54, 73, 84, 85]. As such, the steady state results from the Folgar and Tucker model are selected to base the effectiveness of the proposed model upon. The second-order orientation tensor flow equation of Equation (3.2) with the diffusion model developed of Equation (4.24) is solved using a fourth-order Runge-Kutta solution procedure (see e.g. [76]). As mentioned previously, the fourth- and sixth-order hybrid closures of Advani and Tucker [2] are used to approximate the fourth- and sixth-order orientation tensors respectively, and the eighth- and tenth-order closures from Equations (4.25) and (4.26) are, respectively, used to approximate the eighth- and tenth-order orientation tensors. For each of the following results, the orientation state of the fiber orientation probability distribution will begin from an isotropic orientation state, $\psi(\theta, \phi)$, similar to that of Figure 2.2 with the second-order

orientation tensor A_{ij} given as $A_{11} = A_{22} = A_{33} = \frac{1}{3}$ and $A_{ij} = 0 \forall i \neq j$. It has been shown that flows indicative of those found in industrial applications encounter interaction coefficients of $10^{-4} \leq C_I \leq 10^{-1}$ [3,17,41]. Tucker and Advani [41] discuss a means to relate the volume fraction of fibers V_f to the interaction coefficient C_I , and state that the applicable range of interaction coefficients relates to fiber volume fractions of 10% – 30%.

4.2.4.1 Simple Shear Flow

Simple shear flow often occurs in industrial processes, and regularly serves as the characteristic flow by which the interaction coefficient is based upon [3]. Simple shear flow may be expressed as $v_1 = Gx_3$, $v_2 = v_3 = 0$ and where the flow in the x_1 direction changes in magnitude along the x_3 direction and G is a scaling parameter. The transient solution for simple shear flow from the Folgar and Tucker model for diffusion with an interaction coefficient of $C_I = 10^{-2}$ for $\lambda = 1$ is shown in Figure 4.11. Note this is the same solution as one would obtain using the advanced model for diffusion from Equation (4.24) when $C_1 = 0$ and $C_2 = 10^{-2}$. Observe that the transient results appear to be near the steady state at $Gt = 7 \sim 10$ for each of the components of A_{ij} . It is desired that the proposed model for diffusion will attain similar results for the steady state orientation while approaching the steady state sometime after $Gt = 7 \sim 10$. After several preliminary numerical tests, it was found that a range of coefficients $C_1 \in (0, 4)$ where C_2 was set equal to C_I provided reasonable solutions that were within the expected experimental error (see e.g. [34] for a discussion on experimental difficulties in measuring the orientation state).

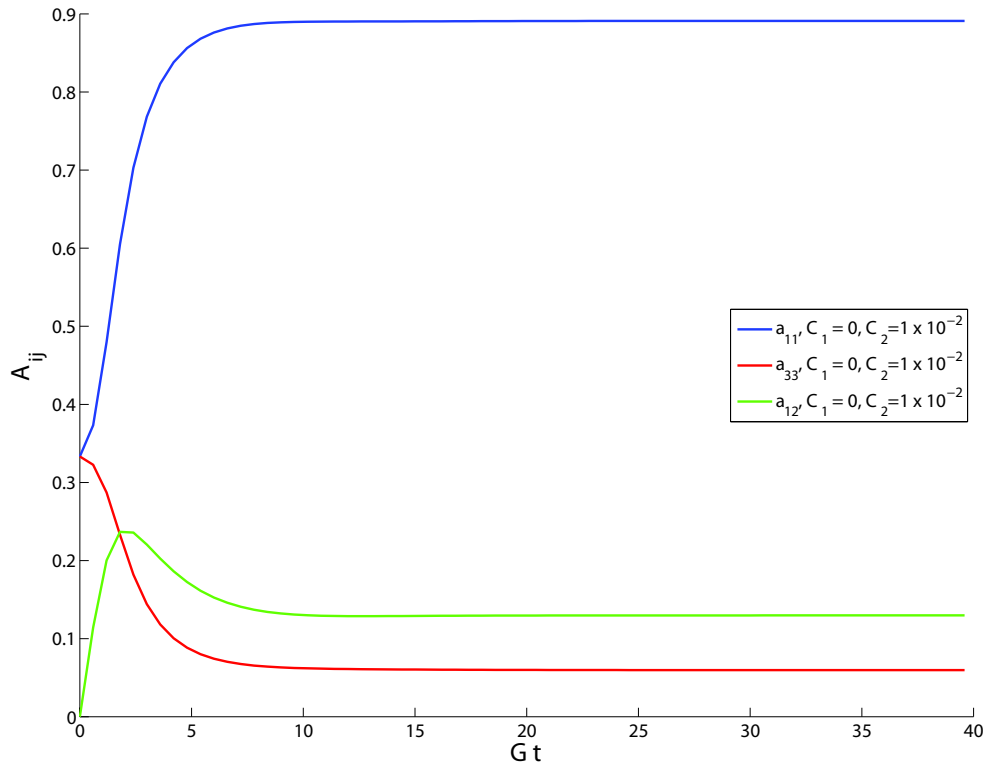


Figure 4.11: Transient solution for A_{ij} from the Folgar and Tucker model in simple shear flow, $v_1 = Gx_3$, $v_2 = v_3 = 0$ starting from an isotropic orientation state, $\psi(\theta, \phi) = \frac{1}{4\pi}$, for $C_I = 10^{-2}$.

The second-order orientation tensor evolution equation was solved using the proposed advanced diffusion model for values of $(C_1, C_2) = (1/2, 10^{-2})$, $(C_1, C_2) = (1, 10^{-2})$, $(C_1, C_2) = (2, 10^{-2})$, and $(C_1, C_2) = (4, 10^{-2})$ and the transient results presented in Figure 4.12. Observe the transient solution from the Folgar and Tucker results given by the solid line compared to the solutions obtained with increasing levels of orientational diffusion. The steady state results for $(C_1, C_2) = (1/2, 10^{-2})$, $(C_1, C_2) = (1, 10^{-2})$, and $(C_1, C_2) = (2, 10^{-2})$ are within what would be considered acceptable experimental errors [3] to the steady state results predicted by the Folgar and Tucker model. The difference between the steady state results for $(C_1, C_2) = (4, 10^{-2})$ and those from the Folgar and Tucker are near the limit of the experimental error, and will warrant further investigation in the following examples. For simple shear flow, the diffusion model clearly approximates the experimental orientation state for a wide range of C_1 values while significantly altering the time when the rate of alignment.

The key observation from Figure 4.12 is the rate of alignment and when steady state orientation is obtained. To numerically attain steady state, the numerical solver for the second-order orientation tensor evolution was run until there was not change in the orientation results at the decimal place given by the numerical precision of the solver (double precision), and the steady state results are labeled as A_{ij}^{ss} . For comparison purposes, the flow is considered to be near steady state when the transient orientation state is within 1% of the steady state orientation, i.e. $|(A_{ij}(t) - A_{ij}^{ss}) / A_{ij}^{ss}| \times 100\% \leq 1\%$. The percentage difference between

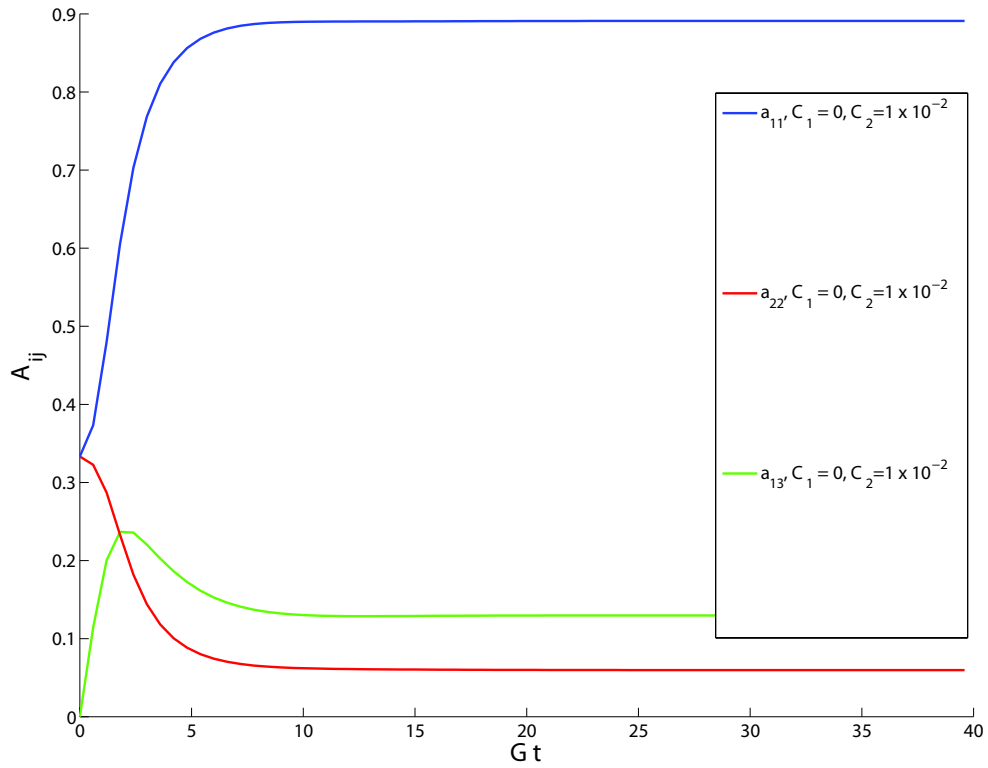


Figure 4.12: Transient solution for A_{ij} from the advanced diffusion model in simple shear flow, $v_1 = Gx_3$, $v_2 = v_3 = 0$ starting from an isotropic orientation state, $\psi(\theta, \phi) = \frac{1}{4\pi}$, with $0 \leq C_1 \leq 4$ and $C_2 = 10^{-2}$.

the transient results and the steady state results for the orientation tensor component A_{11} with diffusion coefficients of $(C_1, C_2) = (0, 10^{-2})$, $(C_1, C_2) = (1/2, 10^{-2})$, $(C_1, C_2) = (1, 10^{-2})$, $(C_1, C_2) = (2, 10^{-2})$ and $(C_1, C_2) = (4, 10^{-2})$ are shown in Figure 4.13. Notice the results from the Folgar and Tucker model given by the line associated with $(C_1, C_2) = (0, 10^{-2})$ reach within 1% of the steady state solution after $Gt \sim 7$. When C_1 increases from 1/2 to 1 to 2 to 4 the results for A_{11} are within 1% of the steady state orientation results after $Gt = 12$, $Gt = 14$, $Gt = 16$ and $Gt = 27$ respectively. These numbers demonstrate a significant alteration of the alignment rate during the transient solution. Recall from the introduction that it is designed to elongate the time required to reach steady state by a factor of 2 to 3 beyond the results predicted by the Folgar and Tucker model. Clearly for select diffusion coefficient C_1 values, the advanced diffusion model falls well within the desired objectives for simple shear flow while retaining the same steady state orientation as predicted by the experimentally fit Folgar and Tucker model.

It was noted that the first-order diffusion model experienced numerical difficulties for large amounts of directional diffusion and high alignment states. It was seen that for alignment states near unidirectional (see e.g. Figure 2.3) the first-order diffusion model would diverge to non-physical orientation states under large values of directional diffusion. This behavior is quite unfortunate, but is not observed in the advanced model for diffusion. Take, for example, the diffusion coefficient pairs $(C_1, C_2) = (1/2, 10^{-2})$ and $(C_1, C_2) = (2, 10^{-2})$ from the initial orientation state nearly unidirectional (see e.g. Figure 2.3) represented by the initial value for the

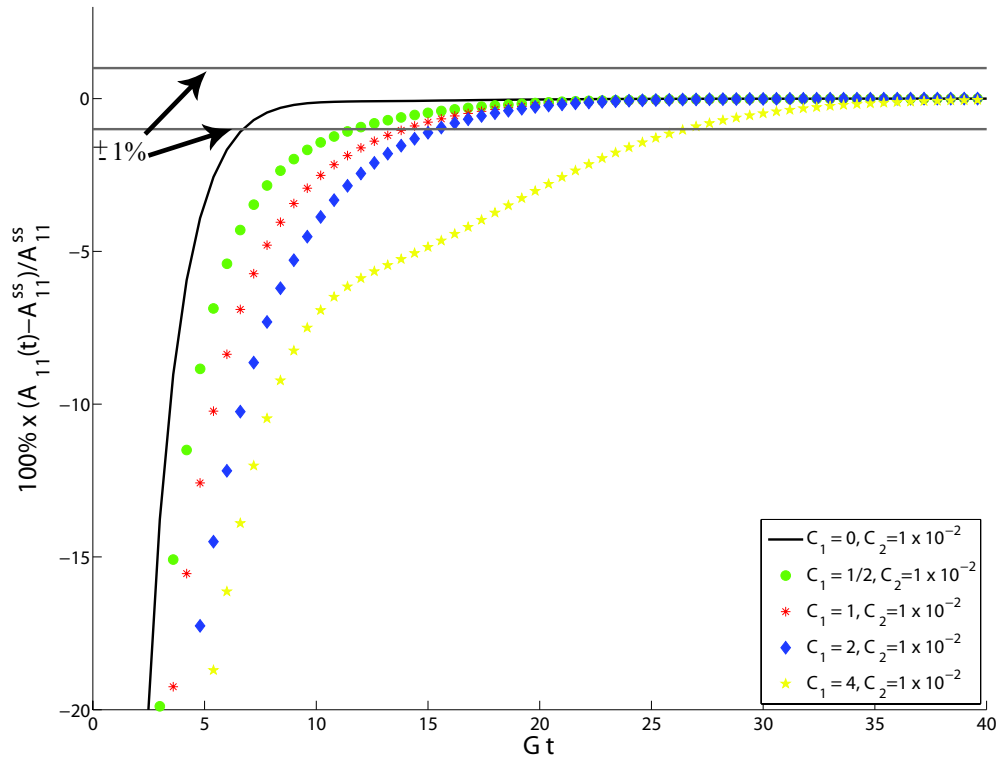


Figure 4.13: Percentage difference between steady state orientation and transient orientation state for A_{11} in simple shear flow, $v_1 = Gx_3$, $v_2 = v_3 = 0$ starting from an isotropic orientation state, $\psi(\theta, \phi) = \frac{1}{4\pi}$, with $0 \leq C_1 \leq 4$ and $C_2 = 10^{-2}$.

second-order orientation tensor $A_{11} = 1 - 10^{-8}$, $A_{22} = A_{33} = \frac{1}{2} \times 10^{-8}$ and $A_{ij} = 0$ $\forall i \neq j$. The preliminary diffusion model will quickly diverge to non-physical results, whereas the advanced diffusion model experiences no such difficulties as evidenced in Figure 4.14. The transient result from an isotropic fiber orientation obtained with the Folgar and Tucker model is shown by the solid line for comparison, observe the advanced diffusion model approaches the same steady state result as in Figure 4.12, beginning from the nearly perfectly aligned orientation state.

4.2.4.2 Uniaxial Elongation Flow

Uniaxial elongation flow is experienced quite often in industrial processes of injection molded parts. Elongational flow will occur when the cavity containing the polymer fluid goes through a rapid expansion. For the following example, the expansion of the bulk fluid motion along the x_1 axis is expanding in the $x_2 - x_3$ plane, and can be characterized by the velocity profile, $v_1 = 2Gx_1$, $v_2 = -Gx_2$ and $v_3 = -Gx_3$ where G is a scaling parameter. Select components of the second-order orientation tensor flow results for $(C_1, C_2) = (0, 10^{-2})$, $(C_1, C_2) = (1/2, 10^{-2})$, $(C_1, C_2) = (1, 10^{-2})$, $(C_1, C_2) = (2, 10^{-2})$ and $(C_1, C_2) = (4, 10^{-2})$ from the advanced diffusion model are presented in Figure 4.15. Observe for diffusion coefficients of $(C_1, C_2) = (1/2, 10^{-2})$ there are minor changes in the orientation characteristics of the results from the Folgar and Tucker model. Conversely, for diffusion coefficients of $(C_1, C_2) = (4, 10^{-2})$ there is a significant change in both the transient solution and in the steady state orientation state. Observe in Figure 4.15 the A_{11} component for $(C_1, C_2) = (4, 10^{-2})$ is well outside the expected error in experimental measurements from the results of the

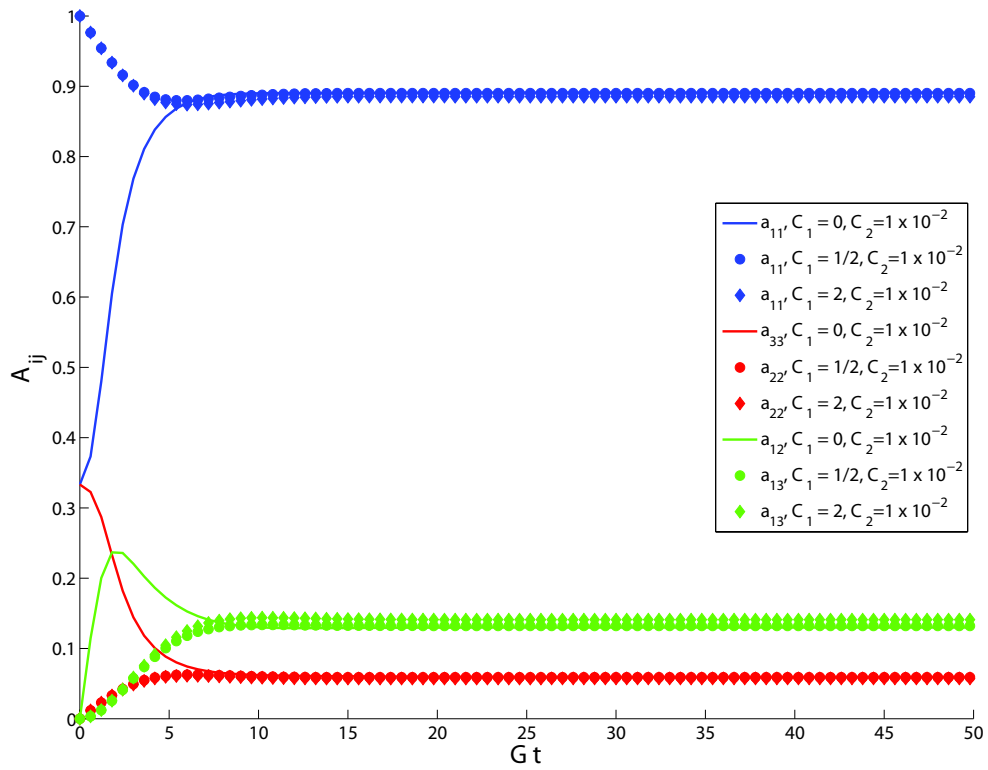


Figure 4.14: Transient solution for A_{ij} from advanced diffusion model in simple shear flow, $v_1 = Gx_3$, $v_2 = v_3 = 0$ starting from a highly aligned orientation state $A_{11} = 1 - 10^{-8}$, $A_{22} = A_{33} = \frac{1}{2} \times 10^{-8}$ and $A_{ij} = 0 \forall i \neq j$.

Folgar and Tucker model. As such the diffusion coefficient pair of $(C_1, C_2) = (4, 10^{-2})$ will be discarded, as well as any value of $C_1 > 4$ when $C_2 = 10^{-2}$. It would be possible to decrease the volume average diffusion effects from C_2 , but it has been observed that this will significantly effect the shape of the steady state fiber orientation probability distribution function $\psi(\theta, \phi)$. Since the only available data comes from the steady state results obtained from the Folgar and Tucker model, deviations from the accepted steady state results would not be prudent without further experimental data. As such, the range of the orientational diffusion coefficient of $0 \leq C_2 \leq 2$ seem to provide steady state orientation results within experimental error of the orientation results from the Folgar and Tucker model while tending to elongate the transient solution. As demonstrated in Figure 4.16 for uniaxial elongation, the time required to approach within 1% of the steady state from the Folgar and Tucker model requires $Gt \sim 0.9$, whereas for diffusion coefficients of $(C_1, C_2) = (1/2, 10^{-2})$, $(C_1, C_2) = (1, 10^{-2})$ and $(C_1, C_2) = (2, 10^{-2})$ it requires, respectively, $Gt \sim 1$, $Gt \sim 1.2$ and $Gt \sim 1.8$.

4.2.4.3 Combined Shearing and Elongational Flow

Typical flows in industrially relevant injection molding processes are not purely shearing or elongational, but a combination of the two flow types. The combined flow chosen has nearly equal shearing and elongation given as $v_1 = Gx_2 - Gx_1$, $v_2 = -Gx_2$ and $v_3 = 2Gx_3$. Observe in Figure 4.17 that the transient solution is significantly altered for the diffusion coefficient pair $(C_1, C_2) = (2, 10^{-2})$ versus that of the results from the Folgar and Tucker model given by the diffusion coefficient pair $(C_1, C_2) = (0, 10^{-2})$. The steady state results are nearly identical, but clearly the transient solution of the

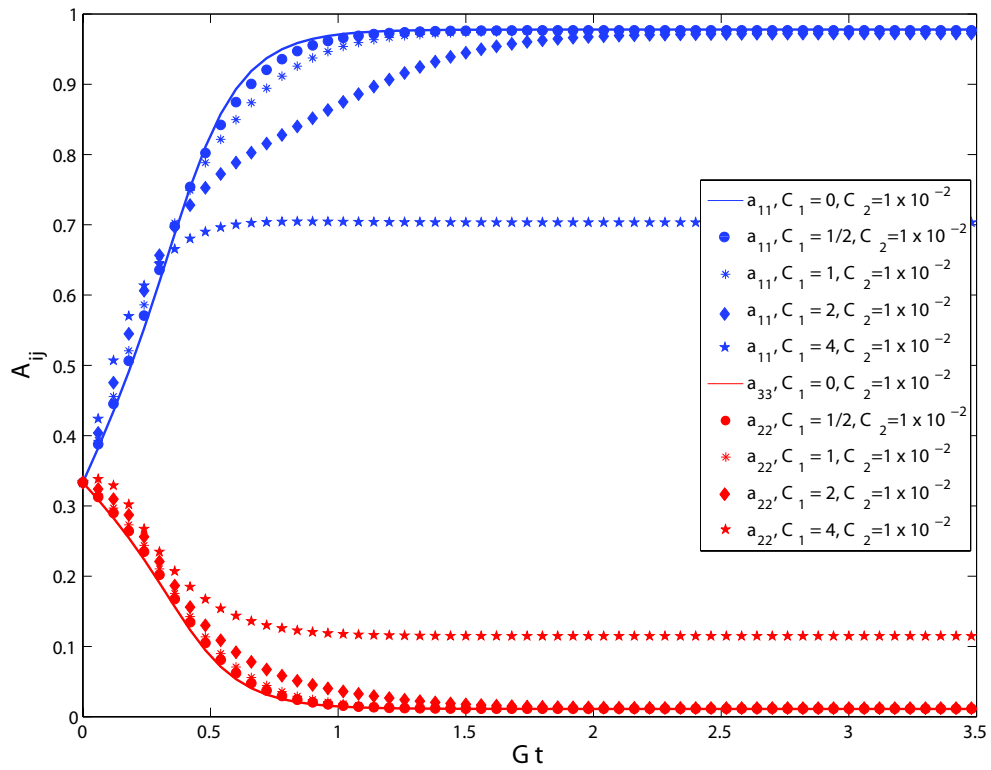


Figure 4.15: Transient solution for A_{ij} from the advanced diffusion model in uniaxial elongational flow, $v_1 = 2Gx_1$, $v_2 = -Gx_2$ and $v_3 = -Gx_3$ starting from an isotropic orientation state, $\psi(\theta, \phi) = \frac{1}{4\pi}$, with $0 \leq C_1 \leq 4$ and $C_2 = 10^{-2}$.

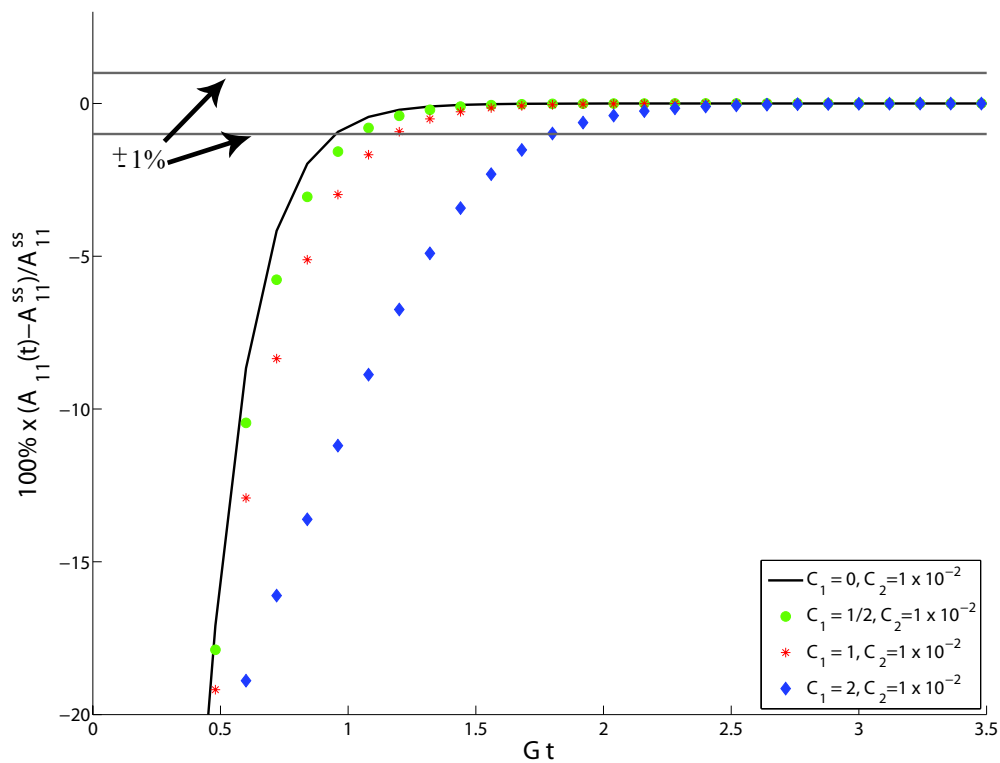


Figure 4.16: Percentage difference between steady state orientation and transient orientation state for A_{11} in uniaxial elongation flow, $v_1 = 2Gx_1$, $v_2 = -Gx_2$ and $v_3 = -Gx_3$ starting from an isotropic orientation state, $\psi(\theta, \phi) = \frac{1}{4\pi}$, with $0 \leq C_1 \leq 2$ and $C_2 = 10^{-2}$.

orientation from the advanced diffusion model follows a significantly different orientation state path to reach steady state than that of the Folgar and Tucker model.

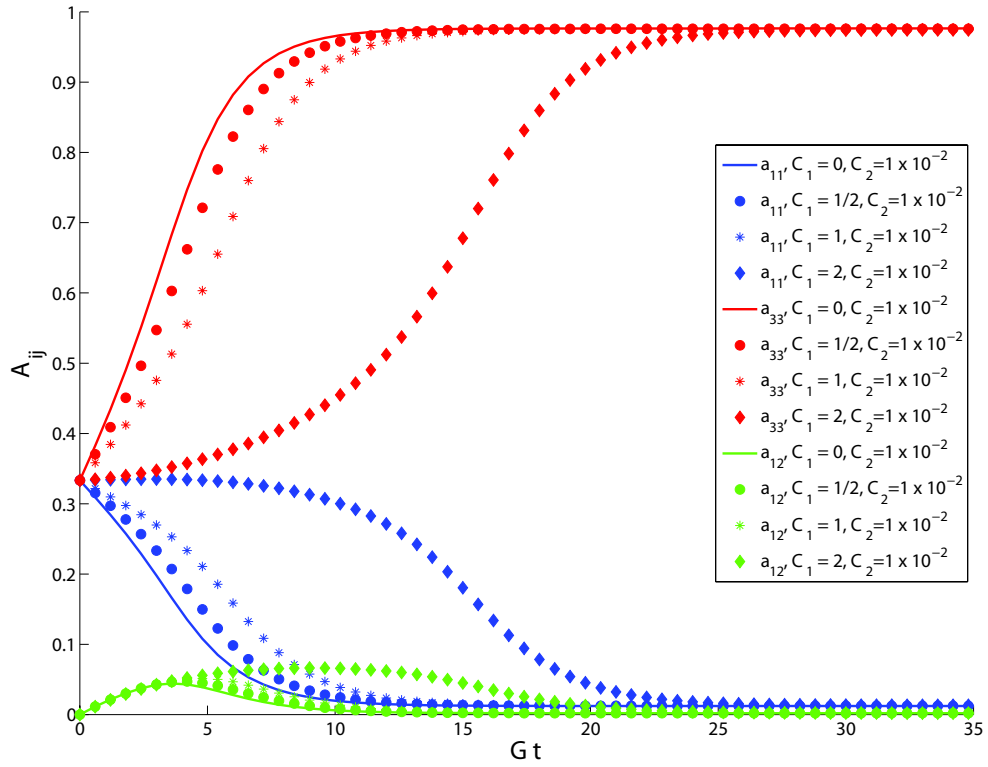


Figure 4.17: Transient solution for A_{ij} from the advanced diffusion model for combined shearing and elongational flow, $v_1 = Gx_2 - Gx_1$, $v_2 = -Gx_2$ and $v_3 = 2Gx_3$ starting from an isotropic orientation state, $\psi(\theta, \phi) = \frac{1}{4\pi}$, with $0 \leq C_1 \leq 2$ and $C_2 = 10^{-2}$.

CHAPTER 5

CONCLUSIONS AND FUTURE WORK

The extensive use of short-fiber reinforced polymer composites in industrial use demands an accurate understanding of the fiber orientation kinematics. In the literature there is a growing concern with the Folgar and Tucker [1] model for fiber interactions to represent an accurate transient analysis of fiber orientation. The Folgar and Tucker model tends to predict an alignment of fibers faster than results viewed in the laboratory environment. Several existing models were discussed that investigate this discrepancy, but each method either focuses on the steady state results or include an empirical time scaling parameter that tends to stretch out the transient solution.

A directionally dependant diffusion model is desired based upon the observation made by Folgar and Tucker in their original work that diffusion effects were different for random orientations versus aligned orientations. It is suspected that due to the significant increase in the capability to model the fiber orientation state made by the Folgar and Tucker theory, a thorough understanding of the physical system was omitted. As the fabrication process has progressed, and products can consistently be manufactured, the demand for an accurate model is necessary.

This work develops the fiber orientation tensor flow equations based upon a directionally dependant diffusion model similar to that of Bird *et al.* [40] that has seen wide use in crystalline polymer flow. This work introduces the advanced directional

diffusion model and provides a means whereby the rate of alignment of the fiber orientation distribution function is altered through a scalable parameter, while retaining the same steady state results as those predicted with current theories. This behavior is quite advantageous since the current theories for fiber interactions are based upon the steady state orientation. The advanced diffusion model presents a set of scalable parameters whereby the time period at which the steady state results are attained may be varied depending upon the physical transient behavior. This will be quite beneficial since the present understanding of the physical characteristics of the transient solution is qualitative in nature. There exists little data available in the literature by which to confirm/deny the present model, and a full investigation of the proposed model will need to incorporate experimental verification. This being considered, the advanced diffusion model satisfies the two principal objectives outlined in the introduction. First, the introduced theory for directional diffusion yields identical steady state results as those obtained with those of the Folgar and Tucker model. Second, the advanced diffusion model provides a means to scale the rate of alignment, and can elongate, in some flows, the transient solution by at least a factor of two in shearing flows and as much as a factor of four in elongational flows.

Future work will need to begin from the fiber orientation probability distribution function evolution equation, and develop a means by which it can be solved. Bay [34] has developed control a volume method to calculate the Folgar and Tucker distribution function evolution, and it is prudent to begin from his foundation. There exist other possible methods to solve the differential equation, such as the finite element method

(see e.g. [86–89]), but difficulties will arise with the higher-order shape functions that will be required to integrate on the surface of the unit sphere.

Additional work should investigate the effects of incorporating fiber interaction effects directly alongside the formulation of the equation of motion of a single fiber. The present work investigated the aspect of the model when fiber interaction effects were assumed to behave as diffusive in nature without fully understand the physical nature between colliding fibers. It is worthwhile to look at the true physical effects when two fibers collide, and how this phenomena is characterized through an investigation of the Jeffery model for non-interacting fibers suspended in a Newtonian fluid.

BIBLIOGRAPHY

- [1] Folgar, F.P. and C.L. Tucker. Orientation Behavior of Fibers in Concentrated Suspensions. *Jn. of Reinforced Plastics and Composites*, **3**:98–119, April 1984.
- [2] Advani, S.G. and C.L. Tucker. The Use of Tensors to Describe and Predict Fiber Orientation in Short Fiber Composites. *Jn. of Rheology*, **31**(8):751–784, 1987.
- [3] Bay, R.S. and C.L. Tucker. Fiber Orientation in Simple Injection Moldings: Part 1 - Theory and Numerical Methods. In *Plastics and Plastic Composites: Material Properties, Part Performance, and Process Simulation, ASME 1991*, volume **29**, pages 445–471. American Society of Mechanical Engineers, 1991.
- [4] Chiba, K., K. Cauda, and K. Natatory. Numerical Solution of Fiber Suspension Flow Through a Parallel Plate Channel by Coupling Flow Field with Fiber Orientation Distribution. *Jn. of Non-Newtonian Fluid Mechanics*, **99**:145–157, 2001.
- [5] Jeffery, G.B. The Motion of Ellipsoidal Particles Immersed in a Viscous Fluid. *Proceedings of the Royal Society of London A*, **102**:161–179, March 1923.
- [6] Advani, S.G. *Prediction of Fiber Orientation During Processing of Short Fiber Composites*. PhD thesis, University of Illinois at Urbana-Champaign, August 1987.
- [7] Hand, G.L. A Theory of Anisotropic Fluids. *Jn. of Fluid Mechanics*, **13**(1):33–46, May 1962.
- [8] Lipscomb, G G II., M.M. Denn, D.U. Hur, and D.V. Boger. Flow of Fiber Suspensions in Complex Geometries. *Jn. of Non-Newtonian Fluid Mechanics*, **26**:297–325, 1988.
- [9] Altan, M.C., S.G. Advani, S.I. Güçeri, and R.B. Pipes. On the Description of the Orientation State for Fiber Suspensions in Homogeneous Flows. *Jn. of Rheology*, **33**(7):1129–1155, 1989.
- [10] Advani, S.G. and C.L. Tucker. Closure Approximations for Three-Dimensional Structure Tensors. *Jn. of Rheology*, **34**(3):367–386, 1990.
- [11] Cintra, J. S. and C.L. Tucker. Orthotropic Closure Approximations for Flow-Induced Fiber Orientation. *Jn. of Rheology*, **39**(6):1095–1122, 1995.
- [12] Dupret, F., V. Verleye, and B. Languillier. Numerical Prediction of the Molding of Composite Parts. In *Rheology and Fluid Mechanics of Nonlinear Materials*, pages 79–90. ASME, 1997.

- [13] VerWeyst, B.E., C.L. Tucker, P.H. Foss, and J.F. O’Gara. Fiber Orientation in 3-D Injection Molded Features: Prediction and Experiment. *International Polymer Processing*, **14**:409–420, 1999.
- [14] Dupret, F. and V. Verleye. Modelling the Flow of Fiber Suspensions in Narrow Gaps. In Siginer, D.A., D.D. Kee, and R.P. Chhabra, editors, *Advances in the Flow and Rheology of Non-Newtonian Fluids, Part B*, pages 1347–1398. Elsevier, Amsterdam, The Netherlands, 1999.
- [15] Petty, C.A., S.M. Parks, and M.S. Shiwei. Flow-Induced Alignment of Fibers. *Proceedings of ICCM-12 Paris, France*, **12**, July 1999.
- [16] Chung, D.H. and T.H. Kwon. Improved Model of Orthotropic Closure Approximation for Flow Induced Fiber Orientation. *Polymer Composites*, **22**(5):636–649, October 2001.
- [17] Chung, D.H. and T.H. Kwon. Invariant-Based Optimal Fitting Closure Approximation for the Numerical Prediction of Flow-Induced Fiber Orientation. *Jn. of Rheology*, **46**(1):169–194, January/February 2002.
- [18] Han, K.-H. and Y.-T. Im. Numerical Simulation of Three-Dimensional Fiber Orientation in Short-Fiber-Reinforced Injection-Molded Parts. *Jn. of Materials Processing Technology*, **124**:366–371, 2002.
- [19] Smith, D.E., B.K. Schache, and D.A. Jack. A Neural Network Based Closure for Modeling Short-Fiber Suspensions. *NSF Design, Service and Manufacturing Grantees and Research Conference*, July 2006.
- [20] Altan, M.C., S. Subbiah, S.I. Guceri, and R.B. Pipes. Numerical Prediction of Three-Dimensional Fiber Orientation in Hele-Shaw Flows. *Polymer Engineering and Science*, **30**(14):848–859, 1990.
- [21] Jack, D.A. and D.E. Smith. An Invariant Based Fitted Closure of the Sixth-order Orientation Tensor for Modeling Short-Fiber Suspensions. *Jn. of Rheology*, **49**(5):1091–1116, September/October 2005.
- [22] Jack, D.A. and D.E. Smith. Sixth-order Fitted Closures for Short-fiber Reinforced Polymer Composites. *Jn. of Thermoplastic Composites*, **19**:217–246, 2006.
- [23] Jack, D.A. and D.E. Smith. The Effect of Fiber Orientation Closure Approximations on Mechanical Property Predictions. *Composites, Part A*, 2006. Accepted for Publication.
- [24] Wright, C. M. Prediction of Elastic Properties and Thermal Expansion for Multi-Component Composites. Master’s thesis, University of Illinois at Urbana-Champaign, Urbana, IL, 1988.

- [25] Camacho, C.W. and C.L. Tucker. Stiffness and Thermal Expansion Predictions for Hybrid Short Fiber Composites. *Polymer Composites*, **11**(4):229–239, August 1990.
- [26] Smith, D.E. and D.A. Jack. Computing Elastic Material Properties From Orientation Tensors. *NSF Design, Service and Manufacturing Grantees and Research Conference*, July 2006.
- [27] Jack D.A. and D.E. Smith. Material Property Predictions for Short-Fiber Polymer Composites: Part 1, Analytical Forms for Expectation and Variance of the Elastic Properties from Orientation Tensors. *Journal of Composite Materials*, 2006. Manuscript Under Review.
- [28] Jack D.A. and D.E. Smith. Material Property Predictions for Short-Fiber Polymer Composites: Part 2, Validation of Analytical Forms of Elastic Properties with the Method of Monte-Carlo. *Composites, Part A*, 2006. *Journal of Composite Materials*.
- [29] Tucker, C.L., J. Wang, J.F. O’Gara, and G. DeBarr. Improved Fiber Orientation Predictions for Injection Molded Composites. In *NSF/DOE/APC Workshop: The Future of Modeling in Composites Molding Processes*, Washington, D.C., June 2004.
- [30] Dinh, S.M. and R.C. Armstrong. A Rheological Equation of State for Semiconcentrated Fiber Suspensions. *Jn. of Rheology*, **28**(3):207–227, 1984.
- [31] VerWeyst, B.E. and Tucker C.L. III. Fiber Suspensions in Complex Geometries: Flow-Orientation Coupling. *The Canadian Journal of Chemical Engineering*, **80**:1093–1106, December 2002.
- [32] Tucker, C.L. Flow Regimes for Fiber Suspensions in Narrow Gaps. *Jn. of Non-Newtonian Fluid Mechanics*, **39**:239–268, 1991.
- [33] Yamane, Y., Y. Kaneda, and M. Dio. Numerical Simulation of Semi-Dilute Suspensions of Rodlike Particles in Shear Flow. *Jn. of Non-Newtonian Fluid Mechanics*, **54**:405–421, 1994.
- [34] Bay, R.S. *Fiber Orientation in Injection Molded Composites: A Comparison of Theory and Experiment*. PhD thesis, University of Illinois at Urbana-Champaign, August 1991.
- [35] Phan-Thien, N., X.-J. Fan, R.I. Tanner, and R. Zheng. Folgar-Tucker Constant for a Fibre Suspension in a Newtonian Fluid. *Journal of Non-Newtonian Fluid Mechanics*, **103**:251–260, 2002.
- [36] Kamal, M.R. and A.T. Mutel. The Prediction of Flow and Orientation Behavior of Short Fiber Reinforced Melts in Simple Flow Systems. *Polymer Composites*, **10**(5):337–343, October 1989.

- [37] Phan-Thien, N., X.-J. Fan, and R. Zheng. Modelling of Viscoelastic Fibre Suspensions. *Unpublished*, 2003.
- [38] Koch, D.L. A Model for Orientational Diffusion in Fiber Suspensions. *Physics of Fluids*, **7**(8):2086–2088, August 1995.
- [39] Bird, R. B., R. C. Armstrong, and O. Hassager. *Dynamics of Polymeric Liquids*, volume 1: Fluid Mechanics. John Wiley & Son, New York, NY, 2nd edition, 1987.
- [40] Bird, R. B., C.F. Curtiss, R. C. Armstrong, and O. Hassager. *Dynamics of Polymeric Liquids*, volume 2: Kinetic Theory. John Wiley & Son, New York, NY, 2nd edition, 1987.
- [41] Tucker, C. L. and S. G. Advani. Processing of Short-Fiber Systems. In S.G. Advani, editor, *Flow and Rheology in Polymer Composites Manufacturing*, pages 147–202. Elsevier Science, Amsterdam, The Netherlands, 1994.
- [42] Ranganathan, S. and S.G. Advani. Characterization of Orientation Clustering in Short-Fiber Composites. *Jn. of Polymer Science: Part B: Polymer Physics*, **28**:2652–2672, 1990.
- [43] Tucker, C.L. and R.B. Dessenberger. Governing Equations for Flow and Heat Transfer in Stationary Fiber Beds. In S.G. Advani, editor, *Flow and Rheology in Polymer Composites Manufacturing*, pages 257–323. Elsevier Science, Amsterdam, The Netherlands, 1994.
- [44] Malvern, L.E. *Introduction to the Mechanics of a Continuous Medium*. Prentice-Hall, Englewood Cliffs, NJ, 1969.
- [45] Jones, R.M. *Mechanics of Composite Materials: Second Edition*. Taylor and Francis, Inc., Philadelphia, PA, 1999.
- [46] Jack, D.A. Investigating the Use of Tensors in Numerical Predictions for Short-Fiber Reinforced Polymer Composites. Master’s thesis, University of Missouri - Columbia, August 2003.
- [47] Jack, D.A. and D.E. Smith. Assessing the Use of Tensor Closure Methods With Orientation Distribution Reconstruction Functions. *Jn. of Composite Materials*, **38**(21):1851–1872, 2004.
- [48] Onat, E.T. Effective Properties of Elastic Materials that Contain Penny Shaped Voids. *International Journal of Engineering Science*, **22**(8-10):1013–1021, 1984.
- [49] Onat, E.T. and F.A. Leckie. Representation of Mechanical Behavior in the Presence of Changing Internal Structure. *Jn. of Applied Mechanics*, **55**:1–10, March 1988.

- [50] Gel'Fand, I.M., R.A. Minlos, and Z.Ya. Shapiro. *Representations of the Rotation and Lorentz Groups and Their Applications*. Pergamon Press Limited, Great Britain, 1963.
- [51] Tucker, C.L. and E. Liang. Stiffness Predictions for Unidirectional Short-Fiber Composites: Review and Evaluation. *Composites Science and Technology*, **59**:655–671, 1999.
- [52] Jack, D.A. and D.E. Smith. A Statistical Method to Obtain Material Properties from the Orientation Distribution Function for Short-Fiber Polymer Composites. *Proceedings of ASME IMECE'05, Orlando, FL*, November 2005.
- [53] Jack, D.A. and D.E. Smith. Statistical Predictions for Short-Fiber Material Property Behavior with the INV₆ Closure. *Proceedings of the 2006 SEM Annual Conference and Exposition*, June 2006.
- [54] Bay, R.S. and C.L. Tucker. Fiber Orientation in Simple Injection Moldings: Part 2 - Experimental Results. In *Plastics and Plastic Composites: Material Properties, Part Performance, and Process Simulation, ASME 1991*, volume **29**, pages 473–492. American Society of Mechanical Engineers, 1991.
- [55] Fan, X.-J., N. Phan-Thein, and R. Zheng. Simulation of Fibre Suspension Flow with Shear-Induced Migration. *Jn. of Non-Newtonian Fluid Mechanics*, **90**:47–63, 2000.
- [56] Pipes, R.B., D.W. Coffin, and S.F. Simacek, P. Shuler. Rheological Behavior of Collimated Fiber Thermoplastic Composite Materials. In S.G. Advani, editor, *Flow and Rheology in Polymer Composites Manufacturing*. Elsevier Science Publishers B. V., Amsterdam, The Netherlands, 1994.
- [57] Chinesta, F. and A. Poitou. Numerical Analysis of the Coupling Between the Flow Kinematics and the Fiber Orientation in Eulerian Simulations of Dilute Short Fiber Suspensions Flows. *The Canadian Journal of Chemical Engineering*, **80**:1107–1114, December 2002.
- [58] Reifschneider, L.G. and H.U. Akay. Applications of a Fiber Orientation Prediction Algorithm for Compression Molded Parts With Multiple Charges. *Polymer Composites*, **15**(4):261–269, August 1994.
- [59] Wetzel, E.D. *Modeling Flow-Induced Microstructure of Inhomogeneous Liquid-Liquid Mixtures*. PhD thesis, University of Illinois at Urbana Champaign, 1999.
- [60] Zhu, Y.T., W.R. Blumenthal, and T.C. Lowe. Determination of Non-Symmetric 3-D Fiber-Orientation Distribution and Average Fiber Length in Short-Fiber Composites. *Jn. of Composite Materials*, **31**(13):1287–1301, 1997.
- [61] Fan, X., N. Phan-Thien, and R. Zheng. A Direct Simulation of Fibre Suspensions. *Jn. of Non-Newtonian Fluid Mechanics*, **74**:113–135, 1998.

- [62] Sepehr, M., P.J. Carreau, M. Grmela, G. Ausias, and P.G. Lafleur. Comparison of Rheological Properties of Fiber Suspensions with Model Predictions. *Jn. of Polymer Engineering*, **24**(6):579–610, 2004.
- [63] Mondy, L.A., H. Brenner, S.A. Altobelli, J.R. Abbott, and A.L. Graham. Shear-Induced Particle Migration in Suspensions of Rods. *Jn. of Rheology*, **38**(2):444–452, March/April 1994.
- [64] Weisstein, E.W. Spherical Coordinates. Technical report, *Mathworld—A Wolfram Web Resource*, <http://mathworld.wolfram.com/SphericalCoordinates.html>, 2006.
- [65] Evans, L.C. *Partial Differential Equations*. Graduate Studies in Mathematics, Volume 19. American Mathematical Society, Providence, RI, 1998.
- [66] Doi, M. Molecular Dynamics and Rheological Properties of Concentrated Solutions of Rodlike Polymers in Isotropic and Liquid Crystalline Phases. *Jn. of Polymer Science Part B Polymer Physics*, **19**:229–243, 1981.
- [67] Yang, Q., X. Chen, and L.G. Tham. Relationship of Crack Fabric Tensors of Different Orders. *Mechanics Reserach Communications*, **31**(6):661–666, November/December 2004.
- [68] Girimaji, S.S. A New Perspective on Realizability of Turbulance Models. *Journal of Fluid Mechanics*, **512**:191–210, 2004.
- [69] Jack, D.A. Orientational Dependant Diffusion for Short-Fiber Composites. Master’s thesis, University of Missouri - Columbia, May 2006.
- [70] Chaubal, C.V. and L.G. Leal. A Closure Approximation for Liquid-Crystalline Polymer Models Based on Parametric Density Estimation. *Journal of Rheology*, **42**(1):177–201, January/February 1998.
- [71] VerWeyst, B.E. *Numerical Predictions of Flow Induced Fiber Orientation in Three-Dimensional Geometries*. PhD thesis, University of Illinois at Urbana Champaign, 1998.
- [72] C. Bingham. An Antipodally Symmetric Distribution on the Sphere. *The Annals of Statistics*, **2**(6):1201–1225, 1974.
- [73] Folgar, F. *Fiber Orientation Distribution in Concentrated Suspensions: A Predictive Model*. PhD thesis, University of Illinois at Urbana-Champaign, 1983.
- [74] Intel Corporation. *Intel[©] Visual Fortran v.9.0, with IMSL Libraries, Professional*, 2006.
- [75] Microsoft Corporation. *Microsoft Visual Studio.NET 2003[©], Professional*, 2003.

- [76] Chapra, S.C. and R.P. Canale. *Numerical Methods for Engineers: With Software and Programming Applications*. McGraw Hill, New York, NY, fourth edition, 2002.
- [77] Griffiths, D.V. and I.M. Smith. *Numerical Methods for Engineers: A Programming Approach*. CRC Press, Boca Raton, FL, 1991.
- [78] Stewart, J. *Multivariable Calculus*. Brooks/Cole Publishing Company, Pacific Grove, CA, Third edition, 1995.
- [79] Weisstein, E.W. Scalar Triple Product. Technical report, *Mathworld—A Wolfram Web Resource*, <http://mathworld.wolfram.com/ScalarTripleProduct.html>, 2006.
- [80] Lai, W.M., D. Rubin, and E. Krempl. *Introduction to Continuum Mechanics*. Butterworth Heinemann Ltd., Burlington, MA, Third edition, 1999.
- [81] Yang, W.-H., D.C. Hsu, and V. Yang. Computer Simulation of 3D Short Fiber Orientation in Injection Molding. *ANTEC 2003 – Proceedings of the 61st Annual Technical Conference and Exhibition*, **49**:651–655, May 2003.
- [82] Haag, R. Optimization of the Warpage of Fiber Reinforced Thermoplastics by Influencing the Fiber Orientation. *ANTEC 2003 – Proceedings of the 61st Annual Technical Conference and Exhibition*, **49**:661–664, May 2003.
- [83] Jack, D.A. and D.E. Smith. Assessing the Use of Tensor Closure Methods with Orientation Distribution Reconstruction Functions. *Proceedings of ASME IMECE'03, Washington, D.C.*, 2003.
- [84] Folgar, F. and C.L. Tucker III. Orientation Behavior of Fibers in Concentrated Suspensions. In *Transport Phenomena in Material Processing*, ASME, volume **10**, pages 105–115, 1983.
- [85] Advani, S.G. and C.L. Tucker. A Numerical Simulation of Short Fiber Orientation in Compression Molding. *Polymer Composites*, **11**(3):164–173, June 1990.
- [86] Hughes, T.J.R. *The Finite Element Method: Linear Static and Dynamic Finite Element Analysis*. Dover Publications, Inc., Mineola, NY, 2000.
- [87] Huebner, K.H., D.L. Dewhirst, D.E. Smith, and T.G. Byrom. *The Finite Element Method for Engineers*. John Wiley & Sons, Inc., New York, NY, 4 edition, 2001.
- [88] Reddy, J.N. and D.K. Gartling. *The Finite Element Method in Heat Transfer and Fluid Dynamics*. CRC Press, Boca Raton, Florida, 2001.
- [89] Reddy, J.N. and D.K. Gartling. *An Introduction to Nonlinear Finite Element Analysis*. Oxford University Press, Oxford, Great Britain, 2004.

VITA

David Abram Jack was born on September 10, 1977 in Niceville, Florida and was homeschooled by his loving parents during most of his preliminary education. While attending the Colorado School of Mines he proposed to and married his best friend, the former Trisha Joy Nadeau of Kittredge, Colorado. David graduated first in his class from the Colorado School of Mines with B.S. degrees in Mechanical Engineering and in Engineering Physics. David followed his advisor Douglas E. Smith from Mines to the University of Missouri - Columbia where he has received an M.S. in Mechanical and Aerospace Engineering. He defended his M.S. thesis in Applied Mathematics in the fall of 2006, and is scheduled to defend his Ph.D. in Mechanical and Aerospace Engineering in the same semester. David is a prolific writer and is the lead author for four published articles in internationally recognized journals as prestigious as the Journal of Rheology and Composites, Part A and currently has two more articles under review. He is the lead author of nine different conference proceedings, and served as co-author for two others. During the evenings and weekends of most of his graduate education, David served as the Scoutmaster for Boy Scout Troop 52 of Columbia, Missouri, and is currently serving as the Assistant Scoutmaster in the same troop.